International Journal of Pharmaceutics 665 (2024) 124720

Contents lists available at ScienceDirect

International Journal of Pharmaceutics

journal homepage: www.elsevier.com/locate/ijpharm

Platelet-cloaked alginate-poly (β-amino ester) a novel platform bioinspired polyelectrolyte nanoparticle for targeted delivery of carboplatin in breast cancer: An *in vitro/in vivo* study

Aliakbar Akbari [a], Jaleh Varshosaz [a,*], Mohsen Minaiyan [b], Parisa Heydari [c], Ardeshir Talebi [d], Mehrnaz Salahi [a], Ali Jahanian Najafabadi [e]

[a] Novel Drug Delivery Systems Research Center, Department of Pharmaceutics, School of Pharmacy and Pharmaceutical Sciences, Isfahan University of Medical Sciences, Isfahan, Iran
[b] Department of Pharmacology, School of Pharmacy and Pharmaceutical Sciences, Isfahan University of Medical Sciences, Isfahan, Iran
[c] Department of Materials Engineering, Isfahan University of Technology, Isfahan 84156-83111, Iran
[d] Department of Clinical Pathology, School of Medicine, Isfahan University of Medical Sciences, Isfahan, Iran
[e] Department of Pharmaceutical Biotechnology, School of Pharmacy and Pharmaceutical Sciences, Isfahan University of Medical Sciences, Isfahan, Iran

ARTICLE INFO

Keywords:
Alginate-poly (β-amino ester) nanoparticles
TNBC
Carboplatin
Platelets
Bioinspired nanomaterials

ABSTRACT

Triple-negative breast cancer (TNBC) has poor prognosis. Carboplatin (Crb) is a widely used chemotherapeutic agent, in TNBC but with serious systemic toxicity and poor tumor targeting. Bioinspired drug-loaded platelets (Plt) and Plt-coated nanocarriers evade macrophage phagocytosis by membrane proteins like CD47. The goal of this study was preparation of a novel alginate-poly (β-amino ester) (PβAE) nanoparticles (NPs) for targeted delivery of Crb to TNBC cells by developing and comparison of two bioinspired carriers of Plt membrane (PltM) coated Crb-loaded alginate-poly (β-amino ester) nanoparticles (PltM@Crb-PβAE-ALG NPs) and Plt loaded Crb (Plt@Crb). The NPs were prepared by ionic gelation and subsequently were coated by platelet membrane using ultra-sonication method. The loading efficiency, release profile, and *in vitro* cytotoxicity of both formulations were evaluated on HUVEC and 4 T1 cells. Additionally, the *in vivo* tumor targeting, therapeutic efficacy, and organ toxicity of the two formulations were assessed in a murine tumor model. Results showed both Plt@Crb and (PltM@Crb-PβAE-ALG NPs) exhibited high drug loading efficiency, sustained release, enhanced cytotoxicity against 4 T1 cells, and decreased cytotoxicity in normal cells (HUVEC) *in vitro*. *In vivo* studies revealed that although both formulations considerably improved tumor inhibition compared to free Crb, but the PltM@Crb-PβAE-ALG NPs demonstrated superior cytotoxicity and therapeutic efficacy, thanks to improved Crb's internalization efficiency, enhanced stability, and controlled release properties.

1. Introduction

Triple-negative breast cancer (TNBC) is a subtype of breast cancer in which the tumor lacks estrogen receptor (ER), progesterone receptor (PgR), and human epidermal growth factor receptor 2 (HER2). This cancer usually has a more aggressive nature than other subtypes of breast cancer and has a high tendency to metastasize to other organs such as the brain, bone, liver, and lung (Ahmad, 2019; Bianchini et al., 2016). As a result, these patients have a poorer prognosis than other breast cancer patients (Zhang et al., 2019).

Although TNBC does not respond well to therapeutic agents, chemotherapy is still the main treatment option used for patients (Bianchini et al., 2016). Therefore, it is very important to maximize the efficacy of chemotherapeutic agents on tumor cells, inhibit drug resistance, and minimize side effects. When other chemotherapeutic options aren't effective, platinum salts may be utilized as the first-line therapy for TNBC.

Studies have shown that platinum salts have a significant ability to treat many malignancies such as colorectal, bladder, testicle, ovary, and breast. However, their use is associated with problems such as

* Corresponding author at: Novel Drug Delivery Systems Research Centre, Department of Pharmaceutics, School of Pharmacy and Pharmaceutical Sciences, Isfahan University of Medical Sciences, Isfahan, PO Box 81745-359, Iran.
E-mail addresses: ali.akbaripharm@gmail.com (A. Akbari), varshosaz@pharm.mui.ac.ir (J. Varshosaz), minaiyan@pharm.mui.ac.ir (M. Minaiyan), parisa82@rocketmail.com (P. Heydari), talebi@med.mui.ac.ir (A. Talebi), mehrnazsasas@yahoo.com (M. Salahi), jahanian@pharm.mui.ac.ir (A. Jahanian Najafabadi).

https://doi.org/10.1016/j.ijpharm.2024.124720
Received 28 April 2024; Received in revised form 9 September 2024; Accepted 13 September 2024
Available online 14 September 2024

nephrotoxicity, tinnitus, hearing toxicity, peripheral nerve toxicity, and drug resistance (de Souza et al., 2013). Crb is a cisplatin analog with less gastrointestinal and renal toxicity but more myelosuppression. TNBC cells mainly have mutations and defects in the BRCA1 gene, which makes them sensitive to chemotherapy agents such as platinum salts that cross-link between DNA strands. Many studies have used NPs to overcome the problems of using platinum salts, increase their durability in cancer tissue, and target them. For example, Crb- poly(lactic-co-glycolic acid) (PLGA) NPs were prepared, and results suggested that the drug's cytotoxic efficacy, and the spectrum of curable tumor cells were highly improved (Sadhukha and Prabha, 2014). Shi et al. (Shi et al., 2018) prepared Crb liposomal formulations with different surface charges with or without pegylation and tested them *in vitro* on F98 glioma cells and *in vivo* on mice carrying F98 cells in the brain. Fe_3O_4-based NPs bonded to Crb prodrug, polycaprolactone NPs (Bragta et al., 2018), chitosan NPs (Khan et al., 2017), PAMAM dendrimers attached to poly aspartic acid (Wang et al., 2017), apoferritin and lactoferritin (Ahmed et al., 2014), mesoporous silica (Qu et al., 2017), polymethyl methacrylate (Shome et al., 2014), lauric acid (Liang et al., 2018), and liposomes (Novohradsky et al., 2018) are among the different nanomaterials reported for Crb delivery.

Although the use of NPs in cancer drug delivery has received much attention nowadays, there are still problems with low biocompatibility and low retention time in the blood circulation system, as well as drug release in unwanted organs (Liang et al., 2018). One of the new ways to overcome these limitations is to use natural body cells or bioinspired carriers for drug delivery (Sarkar et al., 2013). This method makes the therapeutic agent highly biocompatible, and the drug will be less taken up by the liver and spleen tissues. Since it is self-recognized by immune cells, it has low immunogenicity and a high retention time in the blood circulation (Xu et al., 2017). In addition, this drug delivery method allows for a personalized carrier using the patient's cells (Rao et al., 2018). Various cells, including red blood cells, leukocytes, and stem cells, have been studied for this purpose (T. Liu et al., 2019; Rao et al., 2018). Platelets (Plt) are circulating blood cells without a nucleus that have a lifespan of 8–10 days (Lu et al., 2019). The main role of Plt is to form clots and stop bleeding (Du and Chen, 2019). Studies have shown that these cells can accumulate in areas with vascular problems, such as inflammatory environments, hemorrhage, thrombosis, and cancerous tissue, and thus, they can be capable of targeted drug delivery to damaged organs (Xu et al., 2017). Tumor cells can interact with Plt through many signals and receptors (Yang et al., 2017). Due to the presence of P-selectin on Plts surface and P-selectin ligand on cancer cells, αIIbβ3 integrins, fibrinogen, α2β1 integrins, collagen, etc.; activated Plts adhere firmly to cancerous cells (Du and Chen, 2019). Therefore, the use of Plt leads to targeted and smart drug delivery (Sarkar et al., 2013). Drug-loaded Plt and Plt-coated nanocarriers evade macrophage phagocytosis by membrane proteins like CD47. Opsonization by complement or IgG is also inhibited by proteins like CD55 and CD59. Thus, by utilizing Plt as a drug delivery system, chemotherapeutic drugs won't be recognized as foreign bodies in the bloodstream (Lu et al., 2019). Accordingly, various studies have been conducted on the use of Plt, Plt plasma membrane, or their surface proteins to deliver drugs to cancerous cells. Platelet membrane (PltM) cloaking technology is a method in which PltM is coated on the surface of NPs. Coated NPs will simulate the behavior of cell transportation *in vivo*. Wang et al. (Wang et al., 2019) loaded bufalin in chitosan oligosaccharide-PLGA NPs and then coated them with PltM. *In vivo*, results suggested that coating with PltM led to a higher uptake of NPs by hepatoma cells. Although the use of PltM-cloaked NPs has many advantages, there are still some challenges in their use, such as complex preparation procedures and the presence of foreign particles that may cause the activation of the immune system (Xu et al., 2017). Accordingly, some researchers have studied the cytoplasmic drug loading of therapeutic agents in Plt. This drug delivery system exhibits excellent biocompatibility, high half-life, targeted delivery of therapeutic agents to tumor cells (Ahmad, 2019; Bianchini et al., 2016; Xu et al., 2017), high drug loading, and a lower cytotoxic dose of the drug (Bianchini et al., 2016; Xu et al., 2017). However, there are still some contradictions in using whole Plt as a drug delivery system, such as the possibility of exacerbating cancer and thrombosis, low shelf-life, and the probability of unwanted Plt activation (Lu et al., 2019). Since both PltM-coated nanoparticles and drug-loaded Plts have advantages in delivering drugs to the tumor, a study is needed to compare their effectiveness.

PβAEs are a class of synthetic polymers with cationic nature, produced by co-polymerizing di-acrylates and amines. The synthesis of these materials is uncomplicated, and various structural variations can be produced using a wide range of commercially available amine and diacrylate monomers (Shenoy et al., 2005a).

The positively charged polymer has the ability to react easily with molecules that carry a negative charge, such as DNA and RNA, and form a complex known as polyplex. Hence, PβAEs have found extensive use in gene delivery (Sahkulubey Kahveci et al., 2022). However, PβAEs formulations have also been studied for delivery of low molecular weight drugs such as paclitaxel and dexamethasone (Shenoy et al., 2005b).

Studies on biocompatibility and cytotoxicity have indicated that compared to existing cationic polymers like poly(ethyleneimine) and poly(L-lysine), PβAEs are notably less toxic. Moreover, PβAEs undergo degradation in physiological conditions by the hydrolysis of their backbone esters, resulting in the production of small molecular bis (β-amino acid) and diol compounds that are relatively safe for systemic delivery applications (Shenoy et al., 2005b).

The positively charged amino groups in PβAEs can potentially form polyelectrolyte complexes (PECs) with negatively charged materials (Gierszewska et al., 2018). Alginates (Alg) are negatively charged polysaccharides that originate primarily from the cell walls of brown algae. It is a copolymer made up of mannuronic and guluronic acid residues (Gierszewska et al., 2018). Alginate tends to contract at low pH and dissolve at high pH, whereas PβAEs dissolve at low pH and become insoluble at high pH. Therefore, we hypothesized that using PECs of alginate- PβAE may be suitable for achieving a sustained drug delivery system (Niculescu and Grumezescu, 2022).

The hypothesis of this study was that the bioinspired Plt or PltM cloaked novel alginate-PβAEs NPs are efficient carriers for targeted delivery of Crb in TNBC. In addition, until now, there is no report comparing the level of cytotoxicity, cell absorption, and effectiveness of these two forms, i.e., PltM coated NPs and the drug-encapsulated in Plt cytoplasm. Therefore, the biocompatibility and antineoplastic efficacy of these two platforms were investigated and compared both *in vitro* and *in vivo*.

2. Materials and methods

2.1. Materials

Carboplatin (Crb) was provided by Actoverco Pharmaceutical Company (Karaj, Iran), thiazolyl blue tetrazolium bromide (MTT), N, N –dimethylethylenediamine, 1,4-butanediol diacrylate, sodium alginate (ALG) were purchased from Sigma-Aldrich (USA). Protease inhibitor cocktail from Melford (UK), dialysis bags (Mol. Wt. cut-off ~ 12–14 kDa) was from Betagen Co. (Mashhad, Iran). Fetal bovine serum (FBS), Roswell Park Memorial Institute-1640 (RPMI-1640) medium, Dulbecco's Modified Eagle Medium (DMEM), penicillin/streptomycin, trypsin and phosphate buffer solution (PBS) were provided by Bioidea (Iran). NaOH, HCl, and dichloromethane were purchased from Merck Chemical Co. (Germany). Balb/C mice were obtained from Pasteur Institute (Iran), and 4 T1-cells (breast cancer cell line) and HUVEC (Human umbilical vein endothelial cells) were provided by Iranian Biological Research Center (Iran).

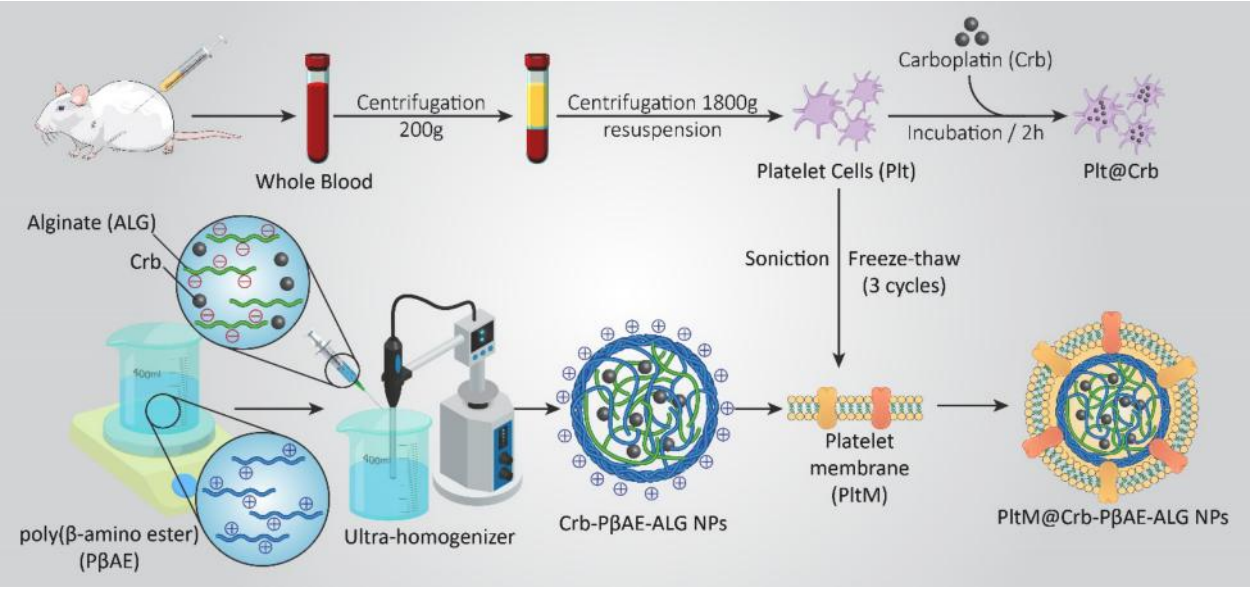

Scheme 1. Schematic illustration of production of Plt@Crb and platelet membrane coated PltM@Crb-PβAE-ALG NPs.

2.2. Plt isolation

To prepare Plt, 9 ml of blood taken from *retro*-orbital vein of rats and 1 ml of 3.2 % sodium citrate solution were mixed. It was centrifuged at 200 g for 10 min at room temperature to obtain platelet-rich plasma (PRP). Then the obtained PRP was centrifuged twice for 20 min at 1800 g, and the supernatant was discarded. The resulting Plt were washed with phosphate-buffered saline (PBS) to obtain pure Plt.

2.3. Drug loading in Plt

Plt@Crb were prepared by dissolving different concentrations of Crb (0.25, 0.5, 1 mg/ml) in PBS and mixed with the Plt (the final Crb concentrations became 0.025, 0.05, 0.1 mg/ml). The resulting mixture was stirred for 1 h at 37 °C in a shaker incubator (GFL 3033, MKS) at 100 rpm.

2.4. Characterization of Plt@Crb

The fresh Plt@Crb suspension was centrifuged at 2000 g for 15 min. The resulting supernatant, which contained unloaded Crb, was gathered, mixed with PBS, and its concentration was determined by spectrophotometer (Shimadzu UV- mini 1240, Japan) at a wavelength of 215 nm (Qu et al., 2017; Xu et al., 2017). By subtracting the amount of free drug from the total initial drug, the amount of loaded drug was obtained. In all stages of the experiment, Plt activation was prevented by 1 mM EDTA. Scanning electron microscopy (SEM, SIGMA, Zeiss, Germany) was used to examine the morphological changes of Plt@Crb. The particle size, zeta potential and polydispersity index of the Plt@Crb in water were analyzed at a temperature of 25 °C using a particle size analyzer (Zetasizer Nano ZS, Malvern Instruments, UK).

2.5. Synthesis of synthesis of poly (β-amino ester)

Synthesis of poly(β-amino ester) (PβAE) was done based on a previous work (Heydari et al., 2023). Briefly, 1,4-butane diol diacrylate and N, N –dimethylethylenediamine were added to dichloromethane in 1:1.1 M ratios and reacted for 48 h at 50 °C on a magnetic stirrer. The resulting polymer was finally washed with diethyl ether and extracted by centrifugation. The successful synthesis of the polymer was shown by ^{1}HNMR (Bruker Biospin, 400 MHz, Germany) and FTIR (FTIR 6300, Jasco, Japan) spectroscopy.

2.6. Preparation and optimization of PβAE-alginate NPs

2.5 ml of sodium alginate (ALG) aqueous solution (pH 5.3) with 1 mg/ml concentration was added drop by drop into 10 ml of PβAE aqueous solution (pH 4.6) with different concentrations (1, 2, 3, 4, 6 mg/ml) under stirring at 13,000 rpm by an ultra-homogenizer (Heidolph, Silent crusher M, Germany). For the preparation of Crb-PβAE-ALG NPs, 4 mg of Crb was dissolved in ALG solution. NPs were optimized based on their particle size, surface charge, and drug loading efficiency, by the method described earlier for Plt@Crb. To check the amount of drug loaded in the NPs, the mixture containing NPs was first centrifuged for 10 min at 12000 rpm, then 1 ml of the supernatant solution was diluted with 19 ml of phosphate buffer (pH 7.4), and its absorbance was read at wavelength of 215 nm spectrophotometrically. NPs were then freeze dried for the next steps.

2.7. PltM coating on NPs

To separate the PltM, first the Plt were prepared according to the method explained earlier in section 2.2. After washing 3 times with PBS, the Plt were suspended in 5 ml PBS containing 1 mM EDTA and 0.5 ml protease inhibitor 10x solution, frozen 3 times in a −80 °C freezer, and thawed again with the help of a bath sonication at room temperature. Then they were centrifuged at 4000 g for 3 min, and the resulting pellets were re-suspended in 2.5 ml PBS containing 1 mM EDTA and 0.25 ml of protease inhibitor 10x solution and sonicated for 5 min with an ultrsonicator probe (Sonicator_3000, Misonix, Inc., Farmingdale, NY, USA) with a power of 60 Watts and a frequency of 40 kHz to obtain platelet membrane (PltM). For preparation of PltM@Crb-PβAE-ALG NPs, 2.5 ml of PBS containing 4 mg of freeze-dried NPs was mixed with the PltM obtained from 5 ml of whole blood. The obtained mixture was sonicated for 5 min with an ultrasonicator-probe with a power of 60 Watts and a frequency of 40 kHz, and finally, their size was reduced by passing through a 0.45 syringe filter (Millipore, Irland) (Wang et al., 2019). Scheme 1 shows the schematic illustration of production of Plt@Crb and PltM@Crb-PβAE-ALG NPs.

To assess the yield of membrane coating on nanoparticles, the absorbance of PltM suspension was initially measured spectrophotometrically at the wavelength of 280 nm before being added to the nanoparticles. After the coating process, the obtained mixture was passed through an Amicon filter and the absorbance of the filtrate (uncoated PltM) was measured at 280 nm. Subsequently, the coating

efficiency was calculated according to the following equation:

$$\text{Coating efficiency\%} = \frac{\text{PltM absorbance at 280nm}}{\text{filtrate absorbance at 280nm}} \times 100 \quad (1)$$

2.8. In vitro Crb release from different formulations

For determining the rate of drug release from Plt@Crb, Crb-PβAE-ALG NPs, and Plt@Crb-PβAE −ALG NPs, 1 ml of the dispersion containing each formulation, was placed in a dialysis bag and the bag was in a saline phosphate buffer (PBS) at a pH of 7.4. Sampling was done at certain time intervals and the samples were quantified spectrophotometrically at a wavelength of 215 nm. Various kinetic models, such as zero order, first order, Higuchi, Hixson-Crowell, and Korsmeyer-Peppas, were employed to investigate drug release kinetics. The most suitable mathematical model determined through curve fitting and correlation coefficient analysis, was chosen to describe the release profile.

$$\text{Zero order}: \ Q_t/Q_\infty = kt \quad (2)$$

$$\text{First order}: \ \text{Ln}(1 - Q_t/Q_\infty) = -kt \quad (3)$$

$$\text{Higuchi}: \ Qt/Q_\infty = kt^{1/2} \quad (4)$$

$$\text{Hixson} - \text{Crowell}: \ Q_0^{1/3} - Q_t^{1/3} = Kt \quad (5)$$

$$\text{Korsmeyer} - \text{Peppas model}: \ Q_t/Q_\infty = kt^n \quad (6)$$

2.9. Cytotoxicity studies

To investigate and compare the cytotoxic effects of the prepared formulations on cancerous and normal cells, MTT assays were performed on 4 T1 cells (TNBC cells) and human umbilical Vein endothelial cells (HUVEC cells) (as a normal cell line). HUVEC and 4 T1 cells were cultured in DMEM and RPMI 1640 mediums respectively, both containing 10 % FBS and 1 % penicillin and streptomycin (100 IU/ml penicillin and 100 μg/ml streptomycin) were kept under conditions of 95 % air and 5 % CO_2 at a temperature of 37 °C. For the MTT test, specific amounts of cells were seeded in the wells of a 96-well plate (1×10^4 for 4 T1 cells and 2×10^4 for HUVEC) and incubated for 24 h. The seeded cells were then treated with 1 μg/ml, 2.5 μg/ml, 10 μg/ml, 25 μg/ml, 50 μg/ml of free Crb, Plt, Plt@Crb, blank and Crb loaded uncoated PβAE-ALG NPs, blank and PltM@Crb-PβAE-ALG NPs, and also a positive control group (only treated with PBS). Cytotoxicity test was performed for 48 h on 2 different days, and each concentration was repeated in 3 wells. 20 Âμl of MTT solution with a concentration of 5 mg/ml in PBS was added to each well, and after 4 h of incubation, the supernatant containing MTT was removed, 180 Âμl of DMSO were added to each well and pipetted slowly to dissolve the formazan crystals. The absorbance of the plates was read by an ELIZA reader (Biotech Instruments, USA) at a wavelength of 570 nm and the percentage of living cells was calculated by the following equation:

$$\text{Cell survival}\ (\%) = \frac{\text{absorbance of test group} - \text{absorbance of blank}}{\text{absorbance of positive control group} - \text{absorbance of blank}} \times 100 \quad (7)$$

To assess the effectiveness and specificity of each treatment in targeting cancer cells, while sparing normal cells, the selectivity index (S.I.) was determined by dividing IC_{50} value of each formulation in normal cells (HUVEC) by the IC_{50} value for the cancer cell line (4 T1) (Calderón-Montaño et al., 2021).

$$\text{S.I} = \frac{\text{IC50 value on HUVEC cells}}{\text{IC50 value on 4T1 cells}} \quad (8)$$

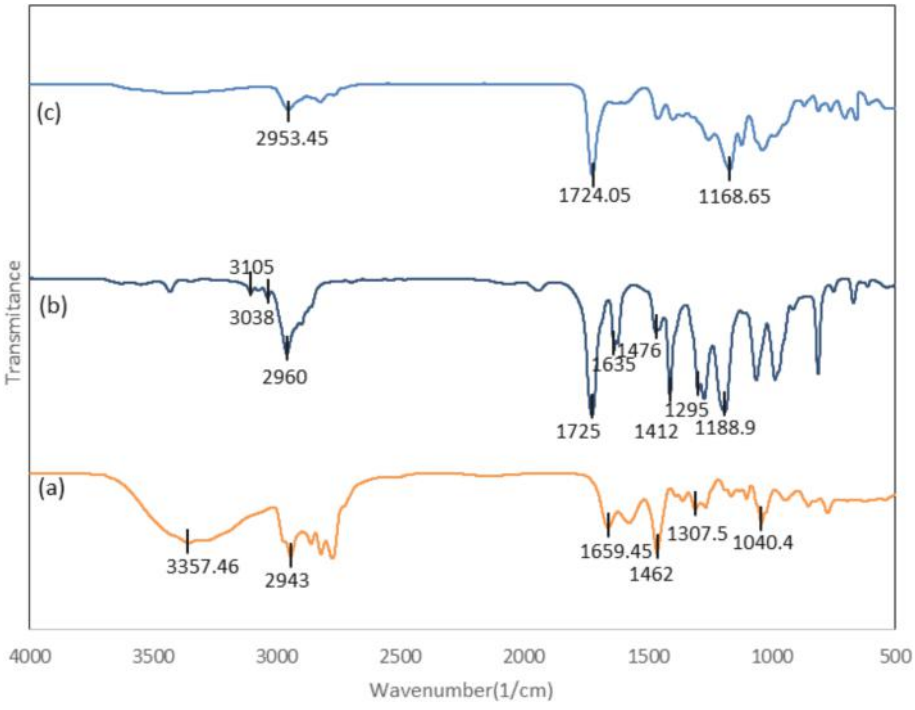

Fig. 1. FTIR spectra of **(a)** N, N-dimethylethylenediamine, **(b)** 1,4-butanediol diacrylate, and **(c)** PβAE.

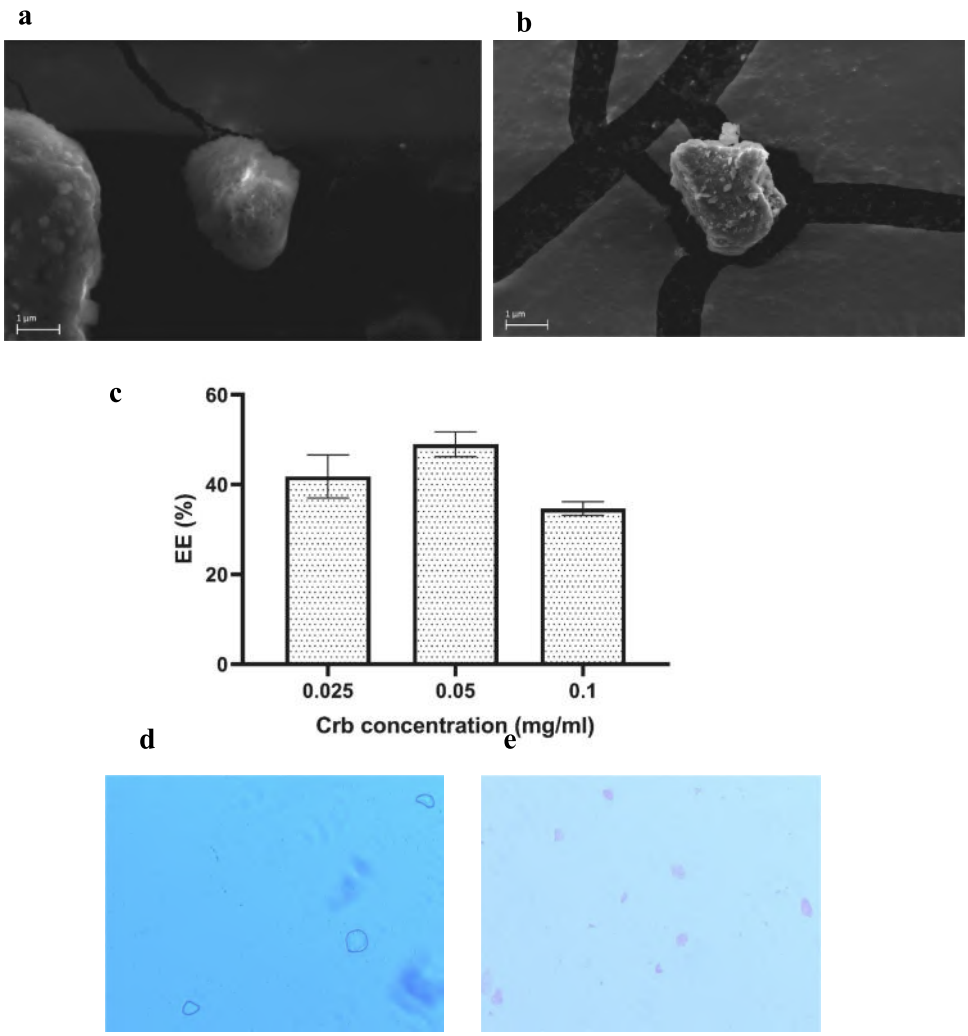

Fig. 2. SEM images of platelets (**a**) before and (**b**) after loading with 0.05 mg/ml Crb. (**c**) Encapsulation efficiency of Crb in Plt@Crb with different concentrations of Crb (0.025, 0.05, and 0.1 mg/ml), and optical image of **(d)** Plts without RhB loading (400 ×) and **(e)** Plts loaded with RhB (400 ×).

2.10. Cellular uptake studies

To investigate and compare cellular uptake of different formulations prepared by cancerous and healthy cells, 4 T1 and HUVEC cells were treated with free Rhodamine B (RhB))as a fluorescent probe instead of Crb), RhB loaded Plts(Plt@RhB), Rhb loaded PβAE-ALG NPs (RhB-PβAE-ALG NPs), and RhB loaded PltM@PβAE-ALG NPs (PltM@RhB-PβAE-ALG NPs) for 4 h. The cells were placed in 6-well plates at a density of 5×10^5 cells per well. Following a 24-hour incubation period at 37 °C with 5 % CO_2 and 95 % humidity, the cells were treated with a 1 μM RhB solution, as well as the same concentration of RhB encapsulated in Plts, NPs and PltM coated NPs for 4 h. Afterward, the cells underwent three washes with PBS to remove the medium and then were quantified using a BD FACSCalibur flow cytometer (Becton Dickinson, USA) (Varshosaz et al., 2019).

2.11. Evaluation of anti-tumor activity and biocompatibility in vivo

BALB/C mice (female, 6–8 weeks old, weight 21–24 g) were obtained from the Pasture Institute (Isfahan, Iran). All experiments were performed under the protocols of the Ethics Committee of Isfahan University of Medical Sciences (ethics code number # IR.MUI.RESEARCH.REC.1399.585). For tumor induction, 2×10^6 4 T1 breast cancer cells were suspended in 0.2 ml of PBS and injected into the right flank of each mouse. When the tumor volume reached 100–200 mm^3, the mice were divided into 6 groups: (i) free Crb (1.8 mg/kg) (ii) uncoated Crb-PβAE-ALG NPs (1.8 mg/kg) (iii) PltM@PβAE-ALG NPs (iv) Plt@Crb (1.8 mg/kg) and (v) PltM@Crb-PβAE-ALG NPs (1.8 mg/kg). Treatments were administered intravenously via the tail vein on days 0, 3, 6, and 9. Tumor size and body weight changes were measured every other day for 6 days when mice were sacrificed (Karimi et al., 2022). The tumor volume measured by a digital caliper was calculated by the following formula:

$$V = \left(L \times W^2\right)/2 \tag{9}$$

where L is the largest diameter and W is the smallest diameter of tumor measured by a caliper. The relative tumor volume (RTV) was calculated with the following equation:

$$RTV = V_f / V_{int} \tag{10}$$

where V_{int} is tumor volume at the first day of experiment and V_f is tumor volume on day 15.

At the end, the tumor, liver, heart, and kidney tissues of animals were collected and fixed in 10 % buffered formalin. At least two samples from each group were embedded in paraffin blocks, then sectioned and stained with hematoxylin and eosin (H&E), and examined using an optical microscope (Olympus CX 21, Japan).

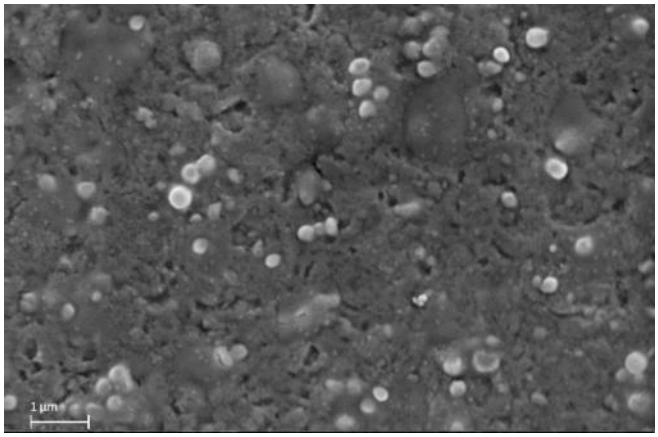

Fig. 3. SEM image of Crb-PβAE-ALG NPs.

3. Results

3.1. Characterization of PβAE

In this study, PβAE was synthesized following the Michael addition reaction mechanism by polymerizing 1,4-butanediol diacrylate and N, N-dimethylethylenediamine stoichiometrically. The polymerization of PβAEs can be carried out in a wide range of solvents. However, dichloromethane was preferred in the synthesis because not only solves the monomers perfectly, but also is easily removed from the reaction media by evaporation.

The FTIR spectra of 1,4-butanediol diacrylate, N, N-dimethylethylenediamine and, PβAE are shown in Fig. 1. In the FTIR spectrum of N, N dimethylethylenediamine (Fig. 1a) at 3357 cm^{-1}, N–H stretching vibrations, N–H bending at 1659.45 cm^{-1}, C–H bending vibrations at 1307.5 and 1462 cm^{-1}, C-N bending vibrations are observed at 1040.4 cm^{-1}, and C–H stretching at 2943 cm^{-1}. In the FTIR spectra of 1,4-butanediol diacrylate (Fig. 1b), stretching C = O bands at 1725 cm^{-1}, C = C stretching at 1635 cm^{-1}, CO stretching at 1295 cm^{-1}, CH bending vibrations of alkane at 1412.6 and 1467.56 cm^{-1}, CH stretching vibrations of alkane at 2960 cm^{-1}, and CH stretching vibrations of alkene at 3105 and 3038 cm^{-1} can be seen. In the PβAE FTIR spectra (Fig. 1c), main peaks are C-O absorption at 1189.9 cm^{-1}, C = O stretching at 1727.9 cm^{-1}, and methyl absorption at 2956.34 cm^{-1}. The removal of the NH peak at 3357.56 cm^{-1}, which is visible in the N, N dimethylethylenediamine (Fig. 1a) and C = C band at 1635 cm^{-1} (Fig. 1b), which are not seen in the PβAE spectra (Fig. 1c), interpreted as the successful synthesis of the polymer.

To further confirmation of the synthesis of PβAE, ^{1}HNMR spectra of monomers and polymer were also recorded. ^{1}HNMR of 1,4-butanediol diacrylate, N, N-dimethylethylenediamine and PβAE are seen in supplementary information.

According to the observed spectrum, the characteristic peaks in N, N-dimethylethylenediamine spectra (Fig. Sa) are 1.71 (br, 2H, NH2), 2.11 (s, 6H, CH3), 2.16–2.25 (m, 2H, NCH2CH2NH2), 2.51–2.58 (m, 2H, NCH2CH2NH2). Characteristic peaks of 1,4-butanediol diacrylate (Fig. Sb) are, 1.68–1.71 (m, 4H, CH2CH2O) (A), 4.12–4.15 (m, 4H, CH2CH2O) (B), 5.92–5.98 (m, 1H, CHCH2) (C), 6.14–6.21 (m, 1H, CHCH2) (C), 6.23–6.37 (m, 1H, CH2) (C). Main peaks in PβAE (Fig. Sc) are 1.62–1.69 (m, A), 2.17 (s, B), 2.37–2.41 (m, C), 2.67–2.70 (m, D), 3.57–3.60 (m, E), 4.01–4.04 (m, G), 4.11–4.15 (m, G), 5.93–6.35 (m, I). The removal of NH peaks and the reduction of the intensity of acrylate peaks confirmed the successful synthesis of the polymer.

3.2. Characterization of Plt@Crb

SEM was used to observe the morphology of Plt before and after the loading of Crb (Fig. 2a, b). Plt@Crb displayed normal shape, indicating that the impact of Crb on the shape of Plt was minimal.

Platelets' capacity to load Crb was assessed by utilizing various ratios of Plt to Crb to create an ideal Plt@Crb delivery system. In the study by Xu et al. (2017), researchers investigated the loading of doxorubicin in platelets across a concentration range of 0.025 to 0.4 mmol/ml and observed that the highest EE% and DL% were obtained in the concentration range of 0.05 to 0.2 mmol/ml. Accordingly, in the present study, we examined the loading of Crb in platelets within a concentration range of 0.0675 to 0.27 mmol/ml (0.025 to 0.1 mg/ml). Centrifugation at 1800 g was used to separate free drug from drug-loaded Plt. The encapsulation efficiency ranged from 34.6 % to 49.0 % in different formulations (Fig. 2c). It was seen that when concentration of Crb was 0.05 mg/ml, the highest encapsulation efficiency obtained and in higher and lower concentrations, EE% was less. To check the drug loading in platelets, platelets were incubated with rhodamine B (RhB) dye instead of Crb. Next, we performed optical imaging of the platelets and the findings were shown in Fig. 2 d, e.

3.3. Preparation and characterization of PβAE-ALG NPs

Crb-PβAE-ALG NPs with different surface charges were prepared by ionic gelation method as a non-toxic, biodegradable, and biocompatible drug delivery system to absorb negatively charged PltM on their surfaces. Crb-PβAE-ALG NPs were easily formed by electrostatic interactions between positively charged PβAE and negatively charged carboxylic groups of ALG. NPs formation was confirmed by scanning electron microscopy (Fig. 3).

The results of encapsulation efficiency, hydrodynamic particle size, polydispersity index, and zeta potential of different formulations are summarized in the Table 1.

As seen in the Table 1, Crb-PβAE-ALG NPs had particle sizes between 265–413 nm. By increasing the amount of PβAE, the drug loading increased and reached a maximum of 69.5 ± 4 % in sample P4A1 but then decreased by increasing above 4 mg/ml in formulation P6A1. As expected, the zeta potential increased with increasing the amount of PβAE and reached a maximum of + 14.00 mV. According to the obtained results, P4A1 was selected for further studies due to higher drug loading efficiency, acceptable PDI and particle size and higher surface charge which was beneficial for more electrostatic conjugation with the PltM.

Successful preparation of Crb-PβAE-ALG NPs was further confirmed by FTIR spectra as seen in Fig. 4. The FTIR of PβAE, sodium ALG, Crb, PβAE-ALG NPs and Crb loaded PβAE-ALG NPs are depicted in this figure. In the PβAE spectrum (Fig. 4a), we can see C-O at 1189.9 cm^{-1}, C = O

Table 1
Physicochemical properties of different Crb-PβAE-ALG nanoparticles.

Formulation	PβAE concentration (mg/ml)	ALG concentration (mg/ml)	Particle size (nm) ± SD	PDI	Zeta potential (mV) ± SD	Crb EE (%)
P1A1	1	1	413.0 ± 28	0.40 ± 0.09	−2.96 ± 0.60	35.0 ± 4
P2A1	2	1	370.2 ± 17	0.31 ± 0.05	+4.93 ± 0.42	40.0 ± 6
P3A1	3	1	265.0 ± 22	0.23 ± 0.06	+9.40 ± 1.70	54.0 ± 8
P4A1	4	1	311.0 ± 34	0.34 ± 0.09	+14.00 ± 0.30	69.5 ± 4
P6A1	6	1	393.8 ± 13	0.80 ± 0.10	+11.45 ± 1.25	61.5 ± 5

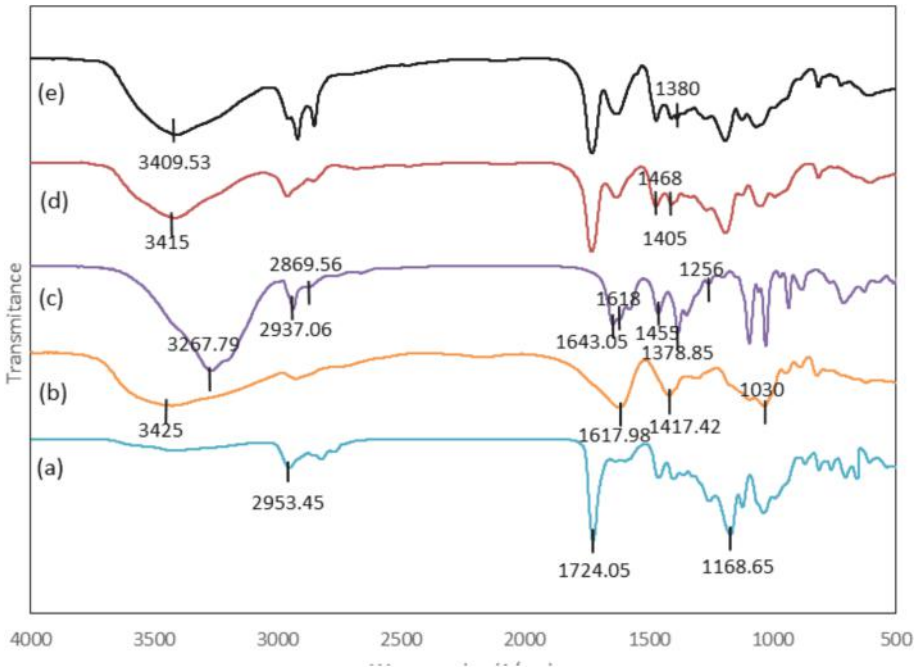

Fig. 4. FTIR spectra of **(a)** PβAE, **(b)** ALG, **(c)** Crb, **(d)** blank PβAE-ALG NPs, and **(e)** Crb-PβAE-ALG NPs.

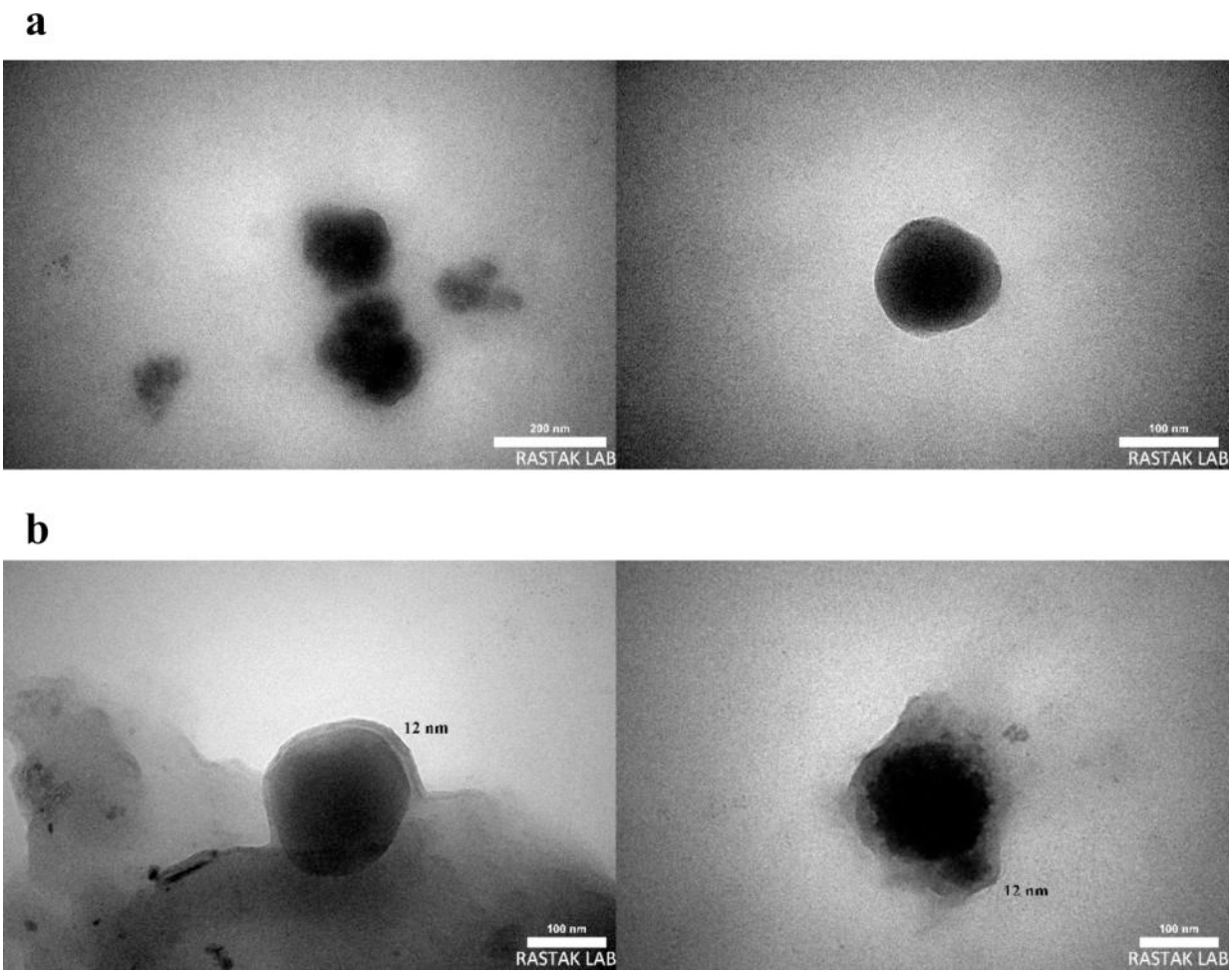

Fig. 5. (**a**) TEM images of Crb-PβAE-ALG NPs and (**b**) PltM@Crb-PβAE-ALG NPs. (**c**) changes of the hydrodynamic diameter of Crb-PβAE-ALG NPs and PltM@Crb-PβAE-ALG NPs in 100% FBS over time and (d) carboplatin release profiles from Plt@Crb, Crb-PβAE-ALG NPs and PltM@Crb-PβAE-ALG NPs.

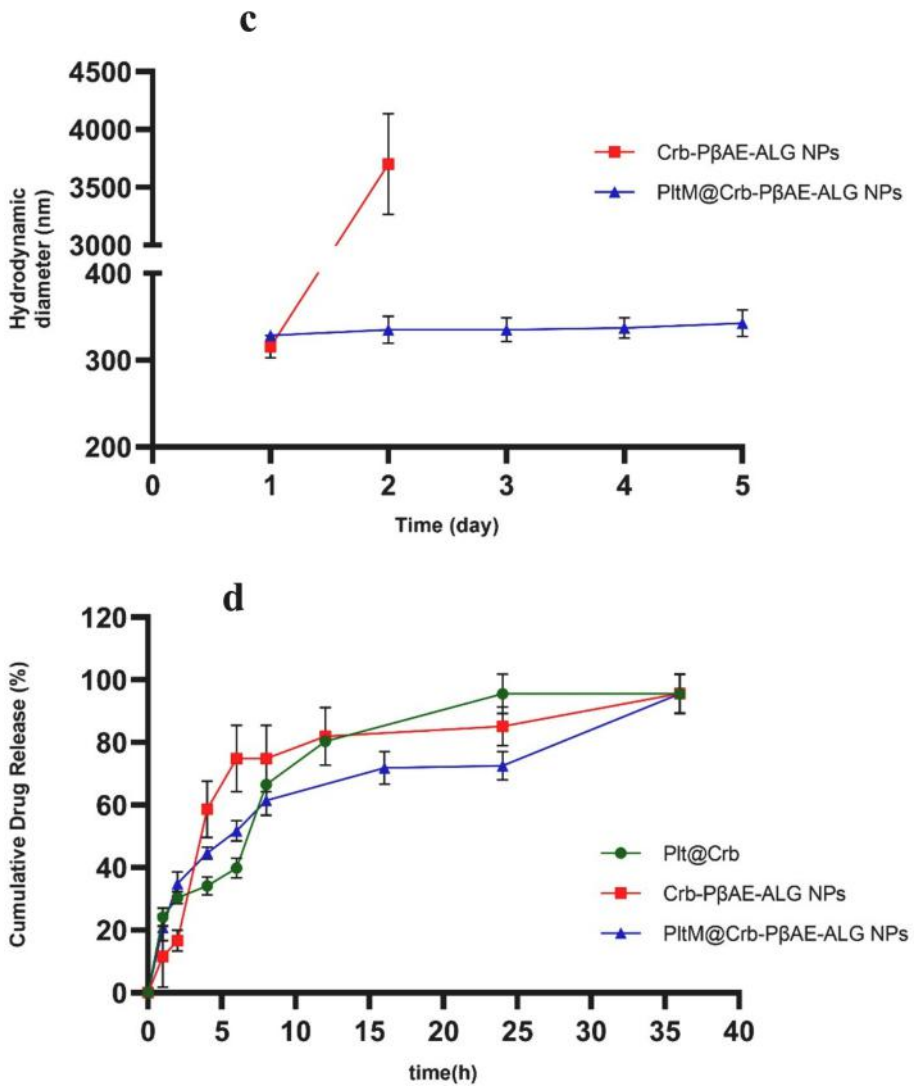

Fig. 5. (*continued*).

stretching at 1727.9 cm^{-1}, methyl absorption at 2956.34 cm^{-1} and N–H bonds at 3432 cm^{-1}. Asymmetric and symmetric stretching vibrations are seen at 1617.98 cm^{-1} and 1417.42 cm^{-1} in the spectrum of ALG (Fig. 4b), due to carboxyl anions, and at 1030 cm^{-1} for oxygen stretching in cyclic ether bridge. The band at 3425 cm^{-1} corresponds to OH stretching vibration. The vibrational bands of the Crb spectrum are seen at 1643.05 cm^{-1}, 3267.79 cm^{-1}, and 1378.85 cm^{-1}, corresponding to C = O, –NH vibration bands, and −C-O of the heterocyclic group, respectively (Fig. 4c). The bands at 2937.06 cm^{-1} and 2869 cm^{-1} correspond to asymmetric and symmetric CH stretching vibrations, respectively (Fig. 4c). Characteristic peaks for the Pt-NH_2 (platinium-amine) bond of Cbr appear at 1378 cm^{-1} and 1256 cm^{-1}. The peaks at 1618 $cm^{-1}$and 1455 cm^{-1} are attributed to the bending vibrations of NH and NH_2, respectively (Fig. 4c).

Blank NPs (Fig. 4d) contain all the main peaks of PβAE. The displacement of the NH peak of PβAE from 3432 cm^{-1} to 3415 cm^{-1} is due to the hydrogen bonding between ALG and the polymer. Additionally, the appearance of the peak at 1405 cm^{-1}, which is not present in pure sodium alginate but is present in the PβAE (Fig. 4a), indicates the formation of a polymer-alginate composite. The peak at 1468 cm^{-1} in the polymer (Fig. 4a) is also not present in pure alginate but is present in the blank NPs, indicating the formation of a composite in the NPs. Finally, in Crb-loaded NPs, we observe the shift of the NH peak of the drug from 3267.79 cm^{-1} (Fig. 4c) to 3409.53 cm^{-1} (Fig. 4e), as well as this peak in the PβAE polymer, which was seen at 3432 cm^{-1} (Fig. 4a) and seen in blank NPs at 3415 cm^{-1} (Fig. 4d) (due to hydrogen bonding between alginate and the polymer) is shifted to 3409.53 cm^{-1} in Crb-PβAE-ALG NPs (Fig. 4e). This indicates the presence of Crb in the NPs and likely hydrogen bonding between the PβAE polymer, ALG, and drug, causes the shift in both combinations. The appearance of a small shoulder in the region of 1380 cm^{-1} related to C-O heterocyclic Crb or its Pt-NH_2 bond that is not observed in any of the spectra of pure polymer and blank NPs, and is now appeared in Crb- PβAE-ALG NPs indicate the presence of drug in NPs.

3.4. Preparation and characterization of PltM@Crb-PβAE-ALG NPs

PltM@Crb-PβAE-ALG NPs were obtained by coating the isolated PltM on the positively charged surface of NPs. The zeta potential results revealed that PltM coating of P4A1 NPs decreased the surface charge from + 14 to −20 mV, which resembled the free platelets. Dynamic light scattering measurement showed that coated NPs had a slightly larger hydrodynamic diameter than uncoated NPs (particle size = 324 ± 8 nm, PDI = 0.47 ± 0.08). The data regarding the dimensions and surface zeta potential indicated that the coating of PβAE-ALG NPs with platelet membrane was successfully done. The coating efficiency was 66.3 ± 8.2 %, which proved the coating of PltM on PβAE-ALG NPs. Transmission electron microscope (TEM) images were also taken to further confirming

Table 2
Correlation coefficient (R^2) of Crb release profile from Plt@Crb, Crb-PβAE-ALG NPs, and PltM@Crb-PβAE-ALG NPs according to different kinetic models.

Formulation	R^2 of different kinetic models					
	Zero order	First order	Higuchi	Hixson-Crowell	Korsmeyer-Peppas	Release exponent (n)
Plt@Crb	0.776	0.9231	0.9285	0.8825	0.9324	0.4071
Crb-PβAE-ALG NPs	0.5648	0.8419	0.7916	0.8935	0.7888	0.6364
PltM@Crb-PβAE-ALG NPs	0.7718	0.9097	0.9417	0.8796	0.9541	0.3835

Table 3
IC_{50} and selectivity index of Crb, Plt@Crb, Crb-PβAE-ALG NPs, PltM@Crb-PβAE-ALG NPs in 24 h and 48 h incubations in HUVEC and 4 T1 cells.

Formulation	IC_{50} (μg/ml) in HUVEC cells		IC_{50} (μg/ml) in 4 T1 cells		Selectivity index	
	24 h	48 h	24 h	48 h	24 h	48 h
Crb	460.3 ± 18.9	433.3 ± 173.2	198.0 ± 5.6	50.6 ± 3.6	2.32	8.57
Plt@Crb	656.0 ± 15.3	610.1 ± 236.5	53.8 ± 0.0	28.1 ± 2.0	12.19	21.72
Crb-PβAE-ALG NPs	97.7 ± 10.1	135.9 ± 31.7	6.5 ± 0.4	6.5 ± 1.0	15.09	20.81
PltM@Crb-PβAE-ALG NPs	272.2 ± 16.8	102.2 ± 8	5.7 ± 0.0	3.0 ± 0.5	47.42	33.79

the lodgment of platelet membranes on the surface of NPs. As can be seen in the Fig. 5, Crb-PβAE-ALG NPs are almost spherical (Fig. 5a). TEM images showed spherical nanoparticles with a core surrounded by a thin layer of PβAE polymer. By coating the platelet membrane on the nanoparticles, a distinct double layer with thickness of 12 nm was lodged on their surface (Fig. 5b).

The stability of Crb-PβAE-ALG NPs and PltM@Crb-PβAE-ALG NPs was tested in simulated blood environment by measuring their hydrodynamic size in 100 % fetal bovine serum (FBS) for 5 days (Xu et al., 2018). As shown in Fig. 5c, the particle size of PltM@Crb-PβAE-ALG NPs exhibited negligible changes in 5 days in 100 % FBS environment, which confirms the stability of PltM@Crb-PβAE-ALG NPs in physiological environment while, Crb-PβAE-ALG NPs showed considerable change in their particle size after 2 days.

3.5. Drug release profiles

The ability of each formulation to control Crb release was assessed using a dialysis bag. The drug release profiles from Plt@Crb, uncoated Crb-PβAE-ALG NPs, and PltM@Crb-PβAE-ALG NPs in phosphate buffer (pH 7.4) are illustrated in Fig. 5d. Plt@Crb and Crb-PβAE-ALG NPs showed a burst release within 4 h, while PltM coating resulted in significant reduction in Crb release of Crb-PβAE-ALG NPs. Plt@Crb had considerable lower burst release compared to Crb-PβAE-ALG NPs and PltM@Crb-PβAE-ALG NPs ($p < 0.05$). However, Crb release from PltM@Crb-PβAE-ALG NPs was significantly lower than Plt@Crb and Crb-PβAE-ALG NPs after 15 and 25 h ($p < 0.05$).

The kinetic of Crb release from different formulations was also studied and as Table 2 shows Crb release from Plt@Crb, and PltM@Crb-PβAE-ALG NPs was fitted with Korsmeyer-Peppas model while, uncoated Crb-PβAE-ALG NPs showed a Hixson-Crowell kinetic model. This model describes the release is controlled by the change in surface area and changes in diameter of the nanoparticles, while Korsmeyer-Peppas model describes the discharge of the drug is controlled by both the Fickian and non-Fickian diffusion mechanism (Mohamed Rizwan and Damodharan, 2020).

3.6. Cell cytotoxicity studies

The cytotoxic effect of the formulations was assessed *in vitro* on 4 T1 and HUVEC cells. Corresponding Crb free formulations were considered as blanks. Table 3 shows the IC_{50} values for both cell lines treated with different formulations. The IC_{50} values in 4 T1 cells after 24 h of treatment showed to be 198.0 ± 5.6, 53.8 ± 0.0, 6.5 ± 0.4, and 5.7 ± 0.0 μg/ml for free Crb, Plt@Crb, Crb-PβAE-ALG NPs, and PltM@Crb-PβAE-ALG NPs, respectively. In addition, the IC_{50} values after 48 h of treatment in 4 T1 cells revealed to be 50.6 ± 3.6, 28.1 ± 2.0, 6.5 ± 1.0, and 3.0 ± 0.5 μg/ml for free Crb, Plt@Crb, Crb-PβAE-ALG NPs, and PltM@Crb-PβAE-ALG NPs, respectively.

Fig. 6 represents findings of the MTT assay results following 24 and 48 h of treatment with the mentioned formulations. As it is shown, blank platelets did not affect cell viabilities significantly following 24 or 48 h treatments, while NP carriers and coated NPs showed significant cytotoxicity at concentrations of 25, 50 μg/ml (according to the Crb concentration).

The cytotoxicity of either Crb or other formulations on HUVECs were also assessed. HUVEC cells, derived from the vein of an umbilical cord, are normal cells that play a crucial role in cardiovascular research and medical investigations (Duranova et al., 2024). In previous studies, these cells have been utilized to investigate cellular toxicity on normal cells and determine selectivity index (Maleki et al., 2021). Besides as we are continuing this study to find the effect of co-targeting triple-negative breast cancer cells and endothelial cells by metronomic chemotherapy to inhibit cell regrowth, anti-angiogenic effect on neovascularization *in vitro* and migration, we chose HUVEC cells, although just the anti-proliferative effects are presented in this article. As it is shown in Fig. 7, at 24 and 48 h of treatment periods, the cytotoxicity of Plt@Crb and PltM@Crb-PβAE-ALG NPs on the 4 T1 cells was significantly higher than on the HUVEC cells ($p < 0.05$). However, the cytolethal effect of the Crb was not significantly different between the two cell lines. For drug-free vehicles, both Plt and PltM@PβAE-ALG NPs showed significantly less cytotoxicity on HUVEC cells compared to 4 T1 cells ($p < 0.05$).

3.7. Cellular uptake

Fig. 8 shows the flow cytometry results after 4 h of incubation of HUVEC and 4 T1 cells with free RhB, RhB loaded platelets (Plt@RhB), RhB loaded NPs (RhB-PβAE-ALG NPs) and RhB loaded in platelet membrane coated NPs (PltM@RhB-PβAE-ALG NPs). This figure shows that cellular uptake of Plt@RhB and PltM@RhB-PβAE-ALG NPs is more than other groups in both cell lines. A more significant shift to the right is observed in the fluorescence signal of all treatments and specially these two formulations in 4 T1 cells compared to HUVEC cells, indicating a higher efficiency of cell harvesting.

3.8. In vivo therapeutic efficacy

The effectiveness of formulations in fighting tumors was studied using a breast tumor bearing mouse model. Throughout the treatment, the mice's weight and tumor dimensions were checked every 3 days. Drug free platelet membrane coated nanoparticles were also used to investigate the biocompatibility of carriers. Fig. 9a shows that the size of tumors in mice treated with PBS and blank Plt coated NPs kept growing. Free Crb group also showed slight growth in tumor size at the end of experiment. For the group treated with Crb-PβAE-ALG NPs no significant change in tumor size was seen at the first three days, but then it began to decrease. Groups treated with Plt@Crb, Crb-PβAE-ALG NPs and

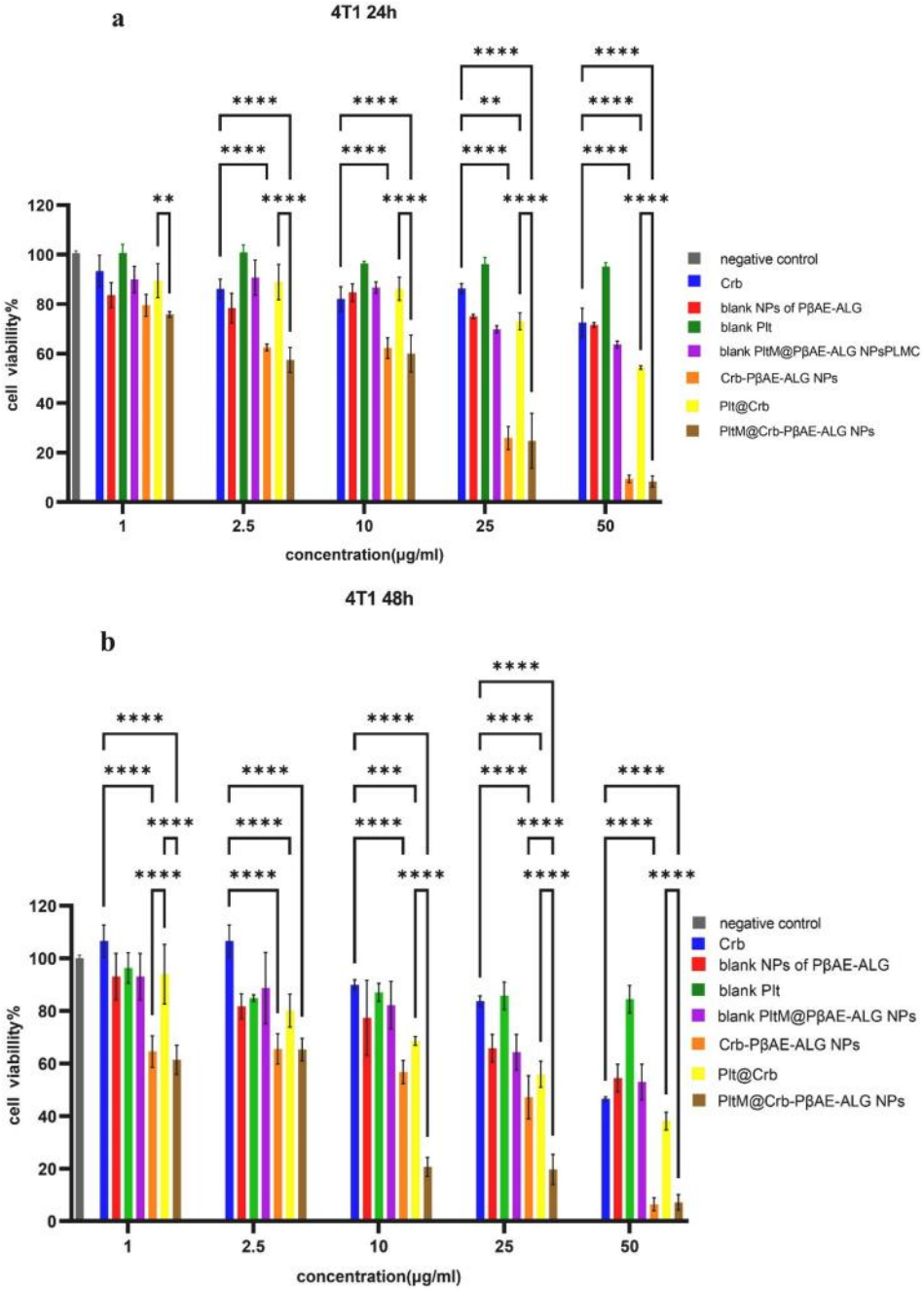

Fig. 6. Cell cytotoxicity on 4 T1 cells after **(a)** 24 h and **(b)** 48 h incubation of free Crb, Blank NPs of PβAE-ALG, Blank Plt, blank PltM@PβAE-ALG NPs, Crb-PβAE-ALG NPs, Plt@Crb, and PltM@Crb-PβAE-ALG NPs. * The mean difference is significant at p value < 0.05, ** p value < 0.01), *** p value < 0.001) and **** p value < 0.0001.

PltM@Crb-PβAE-ALG NPs exhibited a consistent inhibition of tumor growth throughout the experiment and mice treated with PltM@Crb-PβAE-ALG NPs had the highest tumor size reduction at the end of the study. During the study, the alterations in the body mass of mice with breast tumors were documented. The changes in mice body weight are illustrated in Fig. 9b. In PBS and PltM@Crb-PβAE-ALG NPs group we observed around 16.9 and 15.8 percent weight gain, respectively, while all other groups showed decrease in body weight ($p < 0.05$). Mice received free Crb experienced the highest weight loss ($p < 0.05$) and Plt@Crb group had lower weight loss compared to Crb-PβAE-ALG NPs and PltM@Crb-PβAE-ALG NPs at day 15 ($p < 0.05$).

Histopathological changes of tumors and major organs (heart, kidney, liver) examined using hematoxylin-eosin (H&E) staining. As shown in Fig. 9c large number of cancerous cells are seen in PltM@PβAE-ALG NPs and PBS group. In free carboplatin group, a lower cancer cell density is observed. In Crb-PβAE-ALG NPs, Plt@Crb, and PltM@Crb-PβAE-ALG NPs groups, significant reduction of tumor cells and large necrotic tissues was seen. Histopathological images of major organs showed no significant changes in heart and kidney tissues of studied groups (Fig. 9d); However, Crb and Crb-PβAE-ALG NPs groups showed hepatic injuries with necrosis which wasn't seen in Plt@Crb and PltM@PβAE-ALG NPs groups (Fig. 9d) This suggests that Crb encapsulation in Plts or coating of NPs with platelet membrane may protect the liver cells from direct exposure to Crb, potentially reducing its side effects.

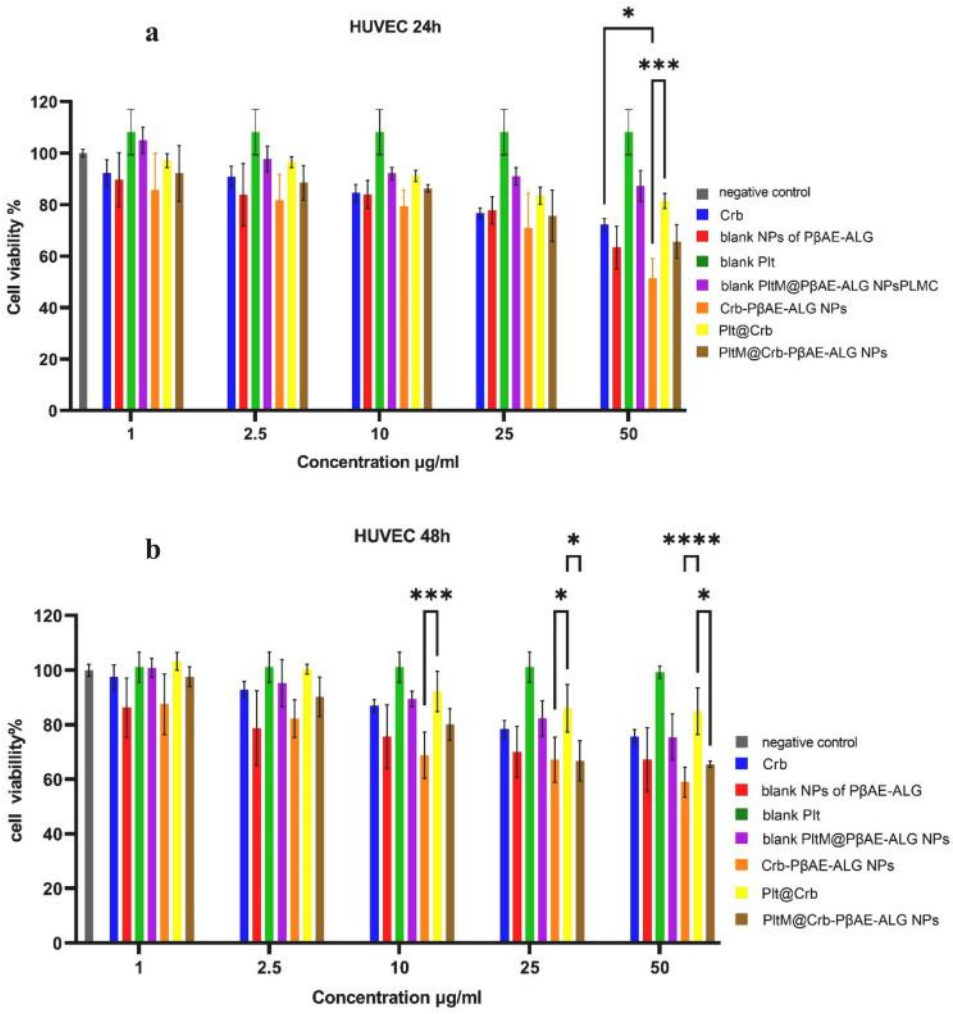

Fig. 7. Cell cytotoxicity on HUVEC after **(a)** 24 h and **(b)** 48 h incubation of free Crb, Blank NPs of PβAE-ALG, Blank Plt, blank PltM@PβAE-ALG NPs, Crb-PβAE-ALG NPs, Plt@Crb, and PltM@Crb-PβAE-ALG NPs.

4. Discussion

Drug delivery using natural biological carriers is a fast-developing field in recent years (Koleva et al., 2020). In this study we developed novel nanoparticles based on polyelectrolyte electrostatic interactions between ALG and PβAE. To target them to TNBC cells the bioinspired platelet coatings were used. Different kinds of cells, such as red blood cells, macrophages, dendritic cells, platelets and stem cells, have been utilized as drug delivery system or have influenced the creation of novel drug delivery systems (Yoo et al., 2011). Among these carriers platelets have gained special interest for cancer drug delivery (Xu et al., 2017). Cancer cells have the tissue factor (a tissue glycoprotein effective in coagulation) on their surface, which can produce thrombin and activate nearby platelets. Activated platelets can interact with cancer cells and play a role in cancer metastasis by aiding the epithelial-mesenchymal transition (EMT) process, protecting circulating tumor cells, and secreting pro-metastatic factors. These interactions between tumor cells and platelets inspired researchers to explore ways to combat cancer using platelet-inspired approaches (Desai et al., 2022). Due to its tendency for frequent relapse and metastasis, which lead to a very poor prognosis TNBC is a challenging issue in clinical settings. Zhang et al (Zhang et al., 2019) developed P-selectin peptide- modified micelles and evaluated their drug targeting, antitumor efficiency and ability to fighting circulating tumor cells. The P-selectin peptide modified micelles have been found to have improved targeting and penetrating capabilities towards primary TNBC and metastasis. This is due to their ability to bind with tumor infiltrating platelets, resulting in a significant improvement in treatment outcomes. Additionally, the micelles have demonstrated a strong ability to suppress lung metastasis of TNBC and reduce the occurrence of distant liver metastasis.

In this study we investigated two drug delivery models inspired by platelets, i.e. direct drug loading into platelets and coating platelet membranes around drug-containing nanoparticles, in terms of their physicochemical properties and efficacy in TNBC treatment.

Platelets have the ability to uptake small molecules and particles (Shattil et al., 1975). The absorption of soluble medications and tiny particles by platelets has been documented (Deb et al., 2011; White, 2005). The important point is that unlike the regular phagocytosis, drug metabolism does not occur in platelets during drug uptake, and for this reason, platelets are called coverocytes (White, 2005). This ability beside platelets ability to target tumor cells made researchers to load anticancer drugs inside platelets. Previous studies reported that platelets have the ability to enclose drugs with a relatively high drug loading capacity (Xu et al., 2017). In this study carboplatin loading in platelets was measured to be ranged from 35 % to 49.5 % (Fig. 2c), while it has no effect on its morphology (Fig. 2a). There were no noticeable changes observed in SEM images (Fig. 2b), indicating that Crb had a negligible effect on the shape of platelets. This was in line with findings of Xu et al (Xu et al., 2017) that loaded doxorubicin in platelets derived from human blood.

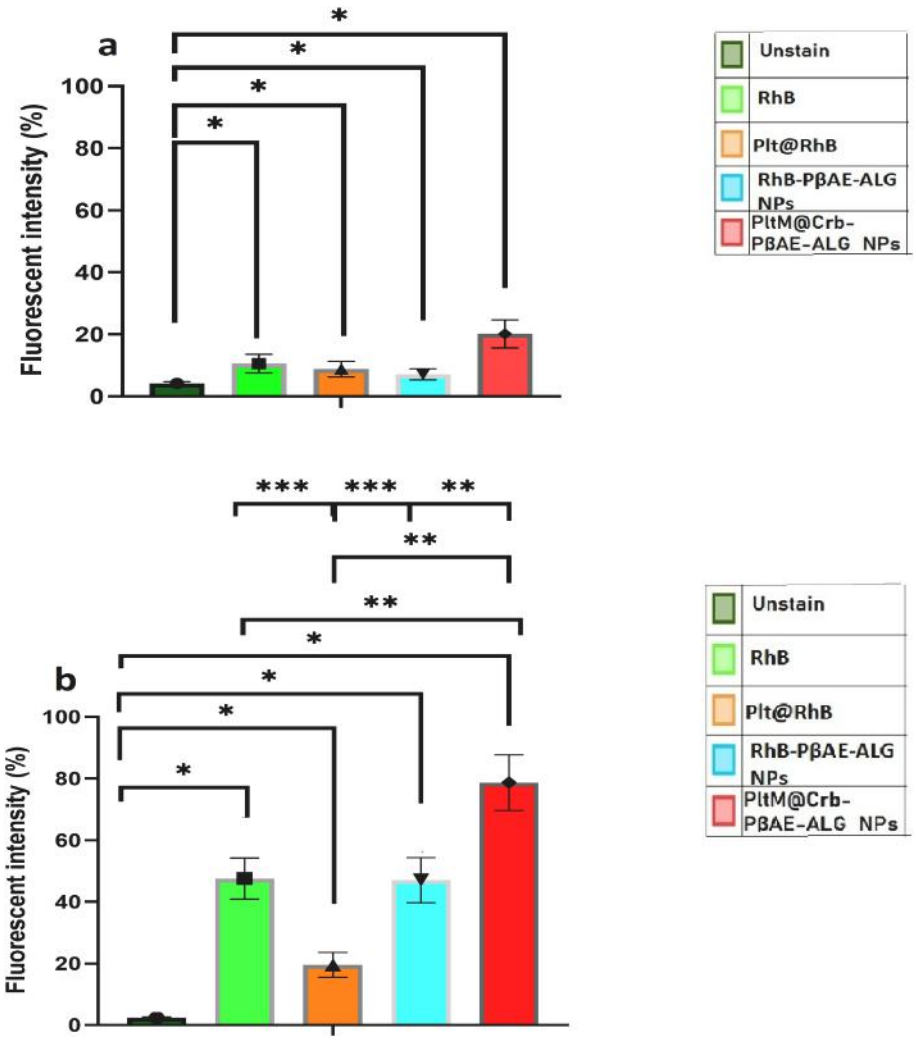

Fig. 8. The results of cellular uptake of free RhB, RhB loaded platelets (Plt@RhB), RhB loaded NPs (RhB-PβAE-ALG NPs) and RhB loaded in platelet membrane coated NPs (PltM@RhB-PβAE-ALG NPs) after 4 h incubation in **a)** HUVEC and **b)** 4 T1 cells shown as fluorescent intensity percent (* The mean difference is significant at p value < 0.05, ** p value < 0.01), *** p value < 0.001).

Polymeric nanoparticles (NPs) and micelles made of polymers have the ability to efficiently load various drugs and transport them to the targeted tumor site, which can enhance the effectiveness of the treatment against the tumor and prevent resistance to multiple drugs in cancer cells. However, these systems may have some disadvantages, including potential toxicity, limited biodegradability, and negative reactions from the immune system (Xu et al., 2017). NPs have a high ratio of surface area to volume due to their nanoscale size, which makes them suitable for surface engineering (Cheng et al., 2021). The initial documentation of the application of cell membrane coating technology on nanoparticles dates back to 2011, when erythrocytes were utilized as a source of coating materials (Hu et al., 2011). By coating cell membrane, nanoparticles gain the ability to mimic normal cells, which is essential for improving drug targeting and enabling further accumulation in specific tissues (Lu et al., 2019).

For preparing PlM@Crb-PβAE-ALG NPs; first the novel PβAE-ALG NPs were fabricated and platelet membrane fragments were coated on them by ultra-sonication. PβAEs are a class of synthetic polycationic polymers prepared by the Michael addition reaction. PβAEs are widely studied for gene delivery due to their good biocompatibility and biodegradability, pH-responsive nature, and easy production (Liu et al., 2019). However, limited studies have evaluated their potential as carriers for other therapeutic agents (Liu et al., 2016; Perni and Prokopovich, 2020). As the pK_a of PβAE is measured to be around 6.5; at a pH around 4.8 amine groups of PβAE become protonated (Liu et al., 2019), and the formation of PβAE-ALG polyionic complex occurs through the ionic interactions between the amine group of PβAE and the carboxylic groups present in ALG. Obtained results suggested that 69.5 % of Crb trapped in this complex (Table 1), which confirmed the formation of NPs.

The FTIR spectra also validated the presence of an electrostatic interaction between amino groups that were protonated and carboxyl groups of ALG (Fig. 4d). Additionally, the spectra indicated that the Crb was present in a chemically stable form within the polymeric matrix (Fig. 4e).

Controlled drug loading and release is beneficial for a drug delivery system because it decreases the required drug dosage, decreases the occurrence of side effects and toxicity, prolongs the duration of therapeutic activity, safeguards sensitive drugs, and enhances the therapeutic impact (Khorshid et al., 2023; Sun et al., 2020). The results demonstrated that while free Crb released within 2 h, encapsulating drug into both PβAE-ALG NPs and platelets prolonged drug release (Fig. 5d). For Crb-PβAE-ALG NPs a rapid burst release was seen within the first 4 h followed by a delayed phase in the next 32 h (Fig. 5d). The sudden release of the drug could be attributed to the Crb being absorbed onto the surface of NPs, whereas the delayed phase may occur due to the trapped drug being released through the diffusion from the matrix (Khan et al., 2017). For PltM@Crb-PβAE-ALG NPs it was noticeable that the

PltM coating reduced the release rate of Crb, indicating that PltM can prevent the burst release of drug from NPs. This was in line with the previous studies conducted by Hu et al (Hu et al., 2015). For Plt@Crb a slower burst release was seen and 33 % of the drug was released within the first 4 h, however, the Plt@Crb continued to release the drug at a higher rate compared to NPs formulations and in 24 h, the amount of drug released was higher than uncoated NPs (Fig. 5d). After 36 h, 94 % of Crb was released from platelets. In the study by Xu et al. (Xu et al., 2017) less than 40 % of the doxorubicin loaded in platelets was released after 36 h. This difference may be due to the higher solubility of Crb compared to doxorubicin in aqueous environment. At the end of 36 h, no significant difference was observed in the amount of released drug from different studied formulations (Fig. 5d).

As a chemotherapy drug, Crb administration is accompanied by significant side effects (Griesinger et al., 2004). Therefore, a drug delivery system that reduces these side effects and improves its therapeutic effectiveness could be a valuable treatment option (Khan et al., 2017). The MTT results indicated that the cytotoxicity of Crb was time-dependent and its IC_{50} enhanced significantly after 48 h incubation (Fig. 6b). Similar results were also obtained for Plt@Crb and Plt@Crb-PβAE-ALG NPs (Fig. 6b). This suggests that longer exposure time may enhance the tumor cells eradication by the medication.

The encapsulated of Crb in platelets and platelet coated NPs resulted in a greater suppression of 4 T1 cells compared to free Crb (Fig. 6b). This implies that a lower dose of Crb can achieve the same therapeutic effect. Hence, normal tissues would be exposed to lower amount of drug, resulting in less side effects (Xu et al., 2017).

Results also revealed that PltM@Crb-PβAE-ALG NPs had the highest cytotoxicity on 4 T1 cells (Fig. 6). This might be due to the combined effects of platelets and NPs, which improved Crb's internalization efficiency (Zhang et al., 2019). The selective cytotoxicity of Plt@Crb and PltM@Crb-PβAE-ALG NPs against tumor cells is a promising result for potential cancer treatments. The fact that these formulations exhibited considerably less cytotoxicity against normal cells (HUVEC) (Fig. 7) suggests that they may cause fewer side effects compared to traditional chemotherapy drugs. This selective cytotoxicity could be attributed to the unique properties of these formulations. In contrast, Crb alone did not show a significant difference in cytotoxicity between HUVEC and 4 T1 cells (Table 3). This further confirms the selective cytotoxicity observed for Plt@Crb and PltM@Crb-PβAE-ALG NPs is not solely due to the Crb, but is rather a result of the combination of Crb with the Plt and PltM coated NP carriers. The selective cytotoxicity of each formulation on cancerous cells was also assessed by calculating the selectivity index (S.I), which also serves as a predictor for their therapeutic value, by comparing their cytotoxic effects on normal and cancerous cells (Krzywik et al., 2020). A higher S.I. indicates greater selectivity towards cancer cells, which is desirable for an effective and safe anticancer agent. The results further confirmed that the encapsulation of Crb into each of

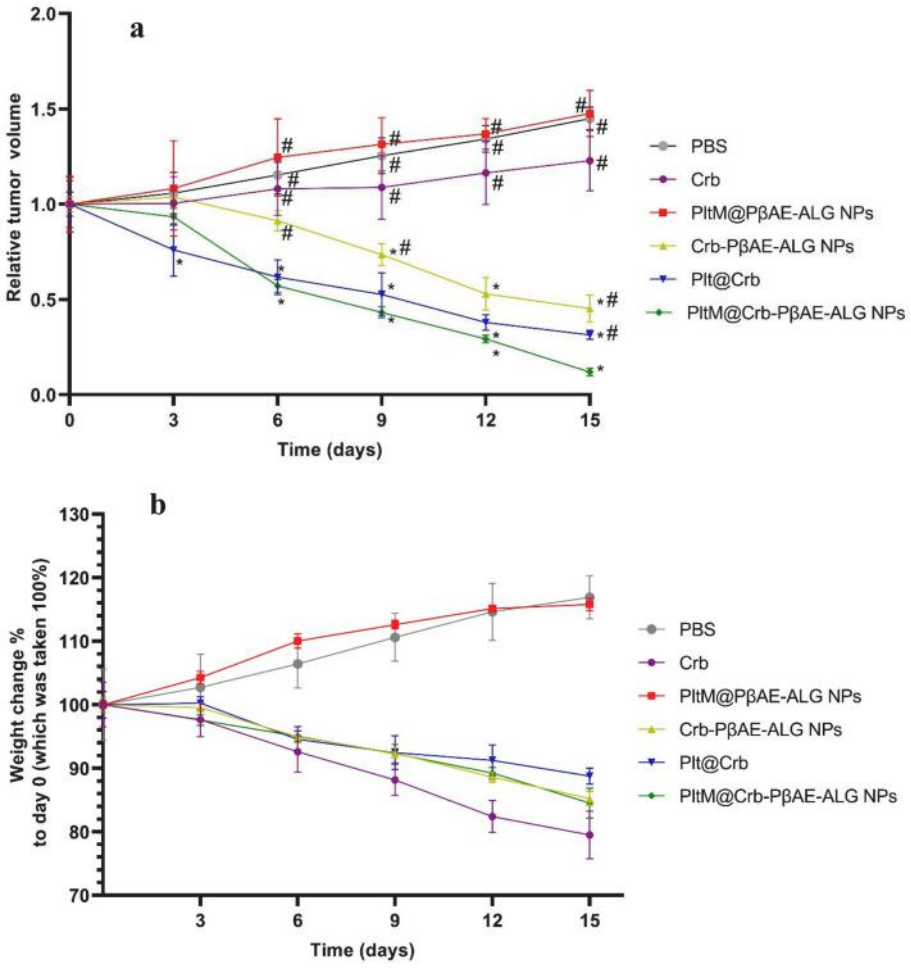

Fig. 9. **(a)** Relative tumor volume (*Significant difference with PBS group (p-value < 0.05), # Significant difference with PltM@Crb-PβAE-ALG NPs group (p-value < 0.05), **(b)** the body weight changes (PBS and PltM@Crb-PβAE-ALG NPs groups although are not different with each other, but have significant difference $p < 0.05$ with other treatments) and **(c)** the H&E staining images (100 ×) of the excised tumor tissues of mice in 15 days after treatment with PBS, PltM@PβAE-ALG NPs, free Crb, Crb-PβAE-ALG NPs, Plt@Crb, and PltM@Crb-PβAE-ALG NPs **(d))** the H&E staining images of the excised heart, kidney, and liver tissues (200 ×) of mice in 15 days after treatment with PBS, PltM@PβAE-ALG NPs, free Crb, Crb-PβAE-ALG NPs, Plt@Crb, and PltM@Crb-PβAE-ALG NPs.

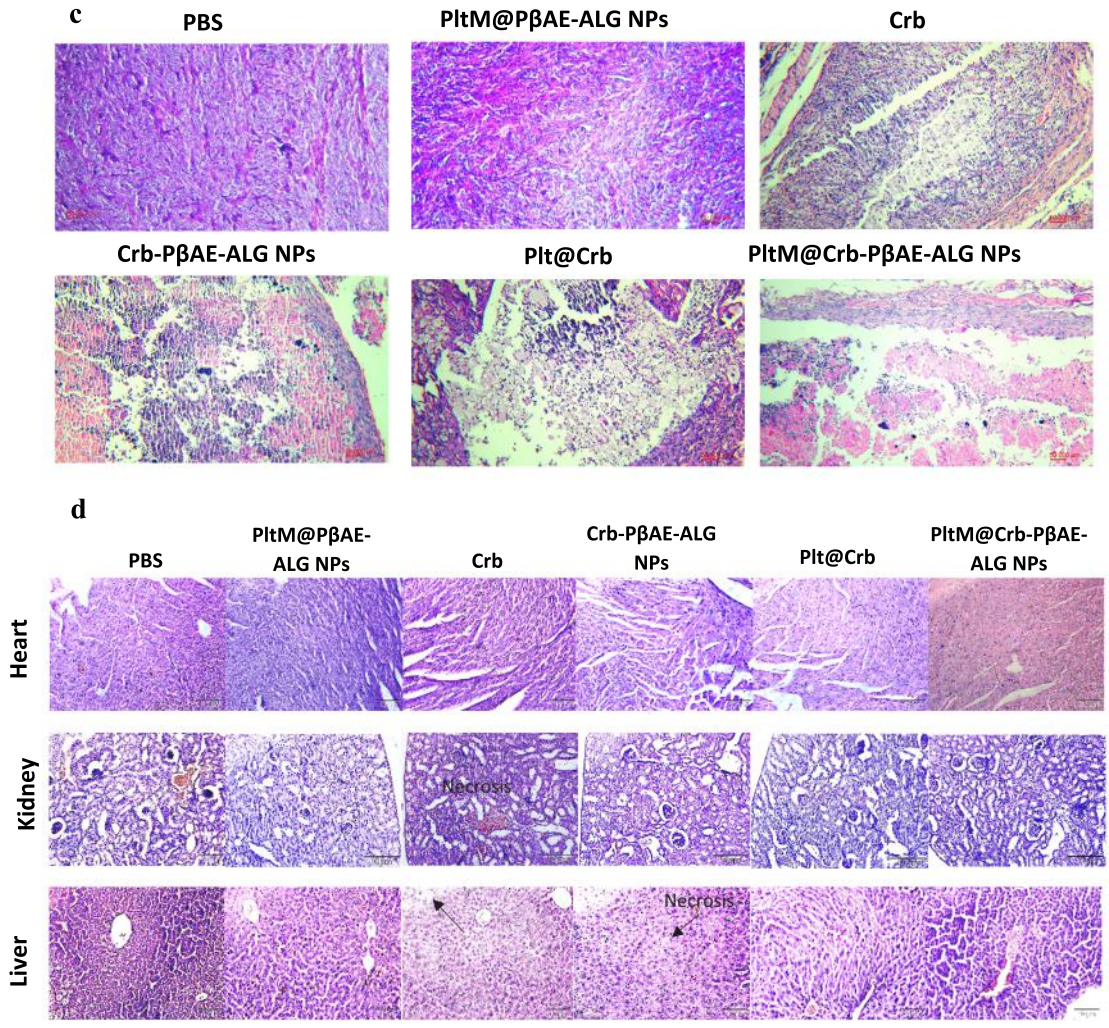

Fig. 9. (*continued*).

the studied carriers, especially nanoparticle-based carriers, and the use of platelet membrane coating can significantly enhance the selectivity of the drug toward cancer cells (Table 3).

The potential reason for the cytotoxicity of PβAE-ALG NPs could be attributed to their positive surface charge. Previous studies have demonstrated that positively charged NPs can harm cell membranes, trigger a stronger immune response, and enhance toxicity in non-phagocytic cells when compared to particles with a neutral or negative charge. However, tumor cells also have a lower uptake of NPs with negative and neutral charge (Bilensoy, 2010). Our results showed that coating platelet membranes on blank PβAE-ALG NPs and Crb- PβAE-ALG NPs led to a significant reduction in cytotoxicity on HUVEC cells (Fig. 7), while higher cytotoxicity on 4 T1 breast cell line was obtained (Fig. 6), which is attributed to the presence of P-selectin protein in Plts effective in their attachment and cellular uptake by 4 T1 cell through overexpressed P-selectin ligand (Du and Chen, 2019). This further proves that the use of cell membranes can improve the biocompatibility and efficacy of nanocarriers (Wang et al., 2019). The results of MTT assay were confirmed by cellular uptake studies carried out by flow cytometry (Fig. 8).

The effectiveness and potential organ toxicity of the treatments were additionally evaluated through tumor bearing mice. As shown in Fig. 9 Crb treated group had less tumor growth compared to blank group ($p < 0.05$). This was consistent with the results obtained by de Souza et al. (de Souza et al., 2013). As shown in Fig. 8a, when mice with tumors were given three different formulations of Crb, there was a significant reduction in tumor growth compared to unloaded Crb at day 15.

The Plt@Crb showed a slightly lower tumor volume than the Crb-PβAE-ALG NPs (Fig. 9a). This could be due to the inherent targeting properties of platelets. However, the difference was not significant ($p > 0.05$), suggesting that both methods are effective in drug delivery (Q. Hu et al., 2015). The PltM@Crb-PβAE-ALG NPs showed the most effective antitumor activity in reducing tumor volume compared to other treatments ($P < 0.05$). This result may indicate that the PltM@Crb-PβAE-ALG NPs have been well mimicked platelets' targeting function (Q. Hu et al., 2015), while cancer cells may internalize the NPs and subsequently break it down to release chemotherapy drugs in the cytosol (Zhang et al., 2019).

Animal weight study revealed that encapsulation of Crb in Plt, coated and uncoated PβAE-ALG NPs led to a significant reduction in weight loss compared to free Crb at day 15 of experiment ($p < 0.05$) (Fig. 9b). This is due to the controlled release and higher targeting ability of formulations, which leads to a lower impact on healthy parts of the body and as a result less systemic toxicity (Karimi et al., 2022).

The H&E staining of tumor sections was used to evaluate the pathological changes of tumors (Fig. 9c). These images showed lower cancerous cell density and angiogenesis in Crb-PβAE-ALG NPs, Plt@Crb and PltM@Crb-PβAE-ALG NPs groups compared to free Crb group. In addition, large apoptic tissue was visible in images of treatment groups. This shows that they have all been able to effectively improve the

delivery of Crb to tumor tissue relative to conventional free Crb solution (Zhang et al., 2019).

5. Conclusion

In the current work, we have successfully developed drug-loaded platelets and platelet membrane coated alginate-poly (β-amino ester) NPs to compare their effectiveness and antitumor effects for delivering Crb to triple-negative cancer cells. By utilizing the particular attraction that exists between cancer cells and platelets, both Plt@Crb and PltM@Crb-PβAE-ALG NPs demonstrated strong antitumor effects with good compatibility. PltM@Crb-PβAE-ALG NPs exhibited higher drug loading and more control over drug release. Additionally, the PltM@Crb-PβAE-ALG NPs had a much greater ability to kill 4 T1 cells than either the free Crb, Crb-PβAE-ALG NPs or the Plt@Crb. Both Plt@Crb and PltM@Crb-PβAE-ALG NPs showed less cytotoxic effects against HUVEC normal cell line. *In vivo* results showed that PltM@Crb-PβAE-ALG NPs could more effectively inhibited tumor growth. In conclusion, this study suggests platelet membrane coated alginate-poly (β-amino ester) NPs as a promising strategy for targeted delivery of Crb in TNBC treatment.

CRediT authorship contribution statement

Aliakbar Akbari: Writing – original draft, Software, Methodology, Investigation, Formal analysis. **Jaleh Varshosaz:** Writing – review & editing, Visualization, Validation, Supervision, Resources, Project administration, Methodology, Funding acquisition, Data curation, Conceptualization. **Mohsen Minaiyan:** Validation, Methodology, Formal analysis. **Parisa Heydari:** Methodology, Investigation. **Ardeshir Talebi:** Methodology, Investigation, Formal analysis, Data curation. **Mehrnaz Salahi:** Investigation, Formal analysis. **Ali Jahanian Najafabadi:** Methodology, Investigation.

Declaration of competing interest

The authors declare that they have no known competing financial interests or personal relationships that could have appeared to influence the work reported in this paper.

Data availability

Data will be made available on request.

Acknowledgments

The financial support of Isfahan University of Medical Sciences (Projects code No.# 399643) is appreciated.

Compliance with ethical standards

Aliakbar Akbari, Jaleh Varshosaz, Mohsen Minayian, Ali Jahanian Najafabadi, Parisa Heydari, Mehrnaz Salahi and Ardeshir Talebi declare that they have no conflict of interest. This article contains animal subjects and animal experiments, which were carried out according to EU Directive 2010/63/EU for animal experiments and approved by the Ethics Committee of Isfahan University of Medical Sciences (Ethical ID: IR.MUI.RESEARCH.REC.1399.585).

Appendix A. Supplementary material

Supplementary data to this article can be found online at https://doi.org/10.1016/j.ijpharm.2024.124720.

References

Ahmed, F., Ali, M.J., Kondapi, A.K., 2014. Carboplatin loaded protein nanoparticles exhibit improve anti-proliferative activity in retinoblastoma cells. Int. J. Biol. Macromol. 70, 572–582.
Bianchini, G., Balko, J.M., Mayer, I.A., Sanders, M.E., Gianni, L., 2016. Triple-negative breast cancer: challenges and opportunities of a heterogeneous disease. Nat. Rev. Clin. Oncol. 13, 674–690.
Bilensoy, E., 2010. Cationic nanoparticles for cancer therapy. Exp. Opin. Drug Deliv. 7, 795–809.
Bragta, P., Sidhu, R.K., Jyoti, K., Baldi, A., Jain, U.K., Chandra, R., Madan, J., 2018. Intratumoral administration of carboplatin bearing poly (ε-caprolactone) nanoparticles amalgamated with in situ gel tendered augmented drug delivery, cytotoxicity, and apoptosis in melanoma tumor. Colloid. Surf. B: Biointerf. 166, 339–348.
Calderón-Montaño, J.M., Martínez-Sánchez, S.M., Jiménez-González, V., Burgos-Morón, E., Guillén-Mancina, E., Jiménez-Alonso, J.J., Díaz-Ortega, P., García, F., Aparicio, A., López-Lázaro, M., 2021. Screening for selective anticancer activity of 65 extracts of plants collected in Western Andalusia. Spain. Plants 10, 2193.
Cheng, Z., Li, M., Dey, R., Chen, Y., 2021. Nanomaterials for cancer therapy: Current progress and perspectives. J. Hematol. Oncol. 14, 1–27.
de Souza, C.M., de Oliveira Gamba, C., de Campos, C.B., Lopes, M.T.P., Ferreira, M.A.N. D., Andrade, S.P., Cassali, G.D., 2013. Carboplatin delays mammary cancer 4T1 growth in mice. Pathol. Res. Practice 209, 24–29.
Deb, S., Patra, H.K., Lahiri, P., Dasgupta, A.K., Chakrabarti, K., Chaudhuri, U., 2011. Multistability in platelets and their response to gold nanoparticles. Nanomed. Nanotechnol. Biol. Med. 7, 376–384.
Desai, C., Koupenova, M., Machlus, K.R., Sen Gupta, A., 2022. Beyond the thrombus: Platelet-inspired nanomedicine approaches in inflammation, immune response, and cancer. J. Thromb. Haemost. 20, 1523–1534.
Du, Y., Chen, B., 2019. Combination of drugs and carriers in drug delivery technology and its development. Drug Des. Devel. Ther. 13, 1401–1408.
Duranova, H., Kuzelova, L., Borotova, P., Simora, V., Fialkova, V., 2024. Human umbilical vein endothelial cells as a versatile cellular model system in diverse experimental paradigms: an ultrastructural perspective. Microsc. Microanal. 30 (3), 419–439.
Gierszewska, M., Ostrowska-Czubenko, J., Chrzanowska, E., 2018. pH-responsive chitosan/alginate polyelectrolyte complex membranes reinforced by tripolyphosphate. Eur. Polym. J. 101, 282–290.
Griesinger, F., Metz, M., Trümper, L., Schulz, T., Haase, D., 2004. Secondary leukaemia after cure for locally advanced NSCLC: alkylating type secondary leukaemia after induction therapy with docetaxel and carboplatin for NSCLC IIIB. Lung Cancer 44, 261–265.
Heydari, P., Varshosaz, J., Kharaziha, M., Javanmard, S.H., 2023. Antibacterial and pH-sensitive methacrylate poly-L-Arginine/poly (β-amino ester) polymer for soft tissue engineering. J. Mater. Sci. Mater. Med. 34, 16.
Hu, C.-M.-J., Zhang, L.i., Aryal, S., Cheung, C., Fang, R.H., Zhang, L., 2011. Erythrocyte membrane-camouflaged polymeric nanoparticles as a biomimetic delivery platform. Proceed. Natl. Acad. Sci. 108, 10980–10985.
Hu, C.-M.-J., Fang, R.H., Wang, K.-C., Luk, B.T., Thamphiwatana, S., Dehaini, D., Nguyen, P., Angsantikul, P., Wen, C.H., Kroll, A.V., 2015a. Nanoparticle biointerfacing by platelet membrane cloaking. Nature 526, 118–121.
Hu, Q., Sun, W., Qian, C., Wang, C., Bomba, H.N., Gu, Z., 2015b. Anticancer platelet-mimicking nanovehicles. Adv. Mater. 27, 7043.
Karimi, Z., Taymouri, S., Minaiyan, M., Mirian, M., 2022. Evaluation of thermosensitive chitosan hydrogel containing gefitinib loaded cellulose acetate butyrate nanoparticles in a subcutaneous breast cancer model. Int. J. Pharm. 624, 122036.
Khan, M.A., Zafaryab, M., Mehdi, S.H., Quadri, J., Rizvi, M.M.A., 2017. Characterization and carboplatin loaded chitosan nanoparticles for the chemotherapy against breast cancer in vitro studies. Int. J. Biol. Macromol. 97, 115–122.
Khorshid, M., Varshosaz, J., Rostami, M., Haghiralsadat, F., Akbari, V., Khorshid, P., 2023. Anti HER-2 aptamer functionalized gold nanoparticles of dasatinib for targeted chemo-radiotherapy in breast cancer cells. Biomater. Adv. 154, 213591.
Koleva, L., Bovt, E., Ataullakhanov, F., Sinauridze, E., 2020. Erythrocytes as carriers: from drug delivery to biosensors. Pharmaceutics 12.
Krzywik, J., Mozga, W., Aminpour, M., Janczak, J., Maj, E., Wietrzyk, J., Tuszyński, J.A., Huczyński, A., 2020. Synthesis, antiproliferative activity and molecular docking studies of novel doubly modified colchicine amides and sulfonamides as anticancer agents. Molecules 25, 1789.
Liang, S., Han, L., Mu, W., Jiang, D., Hou, T., Yin, X., Pang, X., Yang, R., Liu, Y., Zhang, N., 2018. Carboplatin-loaded SMNDs to reduce GSH-mediated platinum resistance for prostate cancer therapy. J Mater. Chem. B. 6, 7004–7014.
Liu, Y., Busscher, H.J., Zhao, B., Li, Y., Zhang, Z., van der Mei, H.C., Ren, Y., Shi, L., 2016. Surface-adaptive, antimicrobially loaded, micellar nanocarriers with enhanced penetration and killing efficiency in staphylococcal biofilms. ACS Nano 10, 4779–4789.
Liu, T., Li, M., Tang, J., Li, J., Zhou, Y., Liu, Y., Yang, F., Gu, N., 2019a. An acoustic strategy for gold nanoparticle loading in platelets as biomimetic multifunctional carriers. J. Mater. Chem. B. 7, 2138–2144.
Liu, Y., Li, Y., Keskin, D., Shi, L., 2019b. Poly (β-Amino Esters): synthesis, formulations, and their biomedical applications. Adv. Healthc. Mater. 8, 1801359.
Lu, Y., Hu, Q., Jiang, C., Gu, Z., 2019. Platelet for drug delivery. Curr. Opin. Biotechnol. 58, 81–91.
Maleki, M., Yazdiniapour, Z., Ghanadian, M., Zolfaghari, B., Rabbani, F., Shafiee, F., 2021. Cytotoxicity and apoptosis inducing effects of some lathyrane and tigliane diterpenes against breast cancer cell lines. Tradit. Integr. Med. 6 (2), 103–110.

Mohamed Rizwan, I., Damodharan, N., 2020. Mathematical modelling of dissolution kinetics in dosage forms. Res. J. Pharm. Tech. 13 (3), 1339–1345.
Niculescu, A.-G., Grumezescu, A.M., 2022. Applications of chitosan-alginate-based nanoparticles—An up-to-date review. Nanomaterials 12, 186.
Novohradsky, V., Zajac, J., Vrana, O., Kasparkova, J., Brabec, V., 2018. Simultaneous delivery of olaparib and carboplatin in PEGylated liposomes imparts this drug combination hypersensitivity and selectivity for breast tumor cells. Oncotarget 9, 28456–28473.
Perni, S., Prokopovich, P., 2020. Optimisation and feature selection of poly-beta-amino-ester as a drug delivery system for cartilage. J. Mater. Chem. B. 8, 5096–5108.
Qu, W., Meng, B., Yu, Y., Wang, S., 2017. EpCAM antibody-conjugated mesoporous silica nanoparticles to enhance the anticancer efficacy of carboplatin in retinoblastoma. Mater. Sci. Eng. C. 76, 646–651.
Rao, L., Bu, L., Ma, L., Wang, W., Liu, H., Wan, D., Liu, J., Li, A., Guo, S., Zhang, L., 2018. Platelet-facilitated photothermal therapy of head and neck squamous cell carcinoma. Angew. Chem. 130, 998–1003.
Sadhukha, T., Prabha, S., 2014. Encapsulation in nanoparticles improves anti-cancer efficacy of carboplatin. AAPS PharmSciTech 15, 1029–1038.
Sahkulubey Kahveci, E.L., Kahveci, M.U., Celebi, A., Avsar, T., Derman, S., 2022. Glycopolymer and Poly (β-amino ester)-Based Amphiphilic Block Copolymer as a Drug Carrier. Biomacromolecules 23, 4896–4908.
Sarkar, S., Alam, M.A., Shaw, J., Dasgupta, A.K., 2013. Drug delivery using platelet cancer cell interaction. Pharm. Res. 30, 2785–2794.
Shattil, S., Anaya-Galindo, R., Bennett, J., Colman, R.W., Cooper, R., 1975. Platelet hypersensitivity induced by cholesterol incorporation. J. Clin. Invest. 55, 636–643.
Shenoy, D., Little, S., Langer, R., Amiji, M., 2005a. Poly (ethylene oxide)-modified poly (β-amino ester) nanoparticles as a pH-sensitive system for tumor-targeted delivery of hydrophobic drugs. 1. In Vitro Evaluations. Mol. Pharm. 2, 357–366.
Shenoy, D., Little, S., Langer, R., Amiji, M., 2005b. Poly (ethylene oxide)-modified poly (β-amino ester) nanoparticles as a pH-sensitive system for tumor-targeted delivery of hydrophobic drugs. In Vitro Evaluations. Mol. Pharm. 2, 357–366.
Shi, M., Anantha, M., Wehbe, M., Bally, M.B., Fortin, D., Roy, L.-O., Charest, G., Richer, M., Paquette, B., Sanche, L., 2018. Liposomal formulations of carboplatin injected by convection-enhanced delivery increases the median survival time of F98 glioma bearing rats. J. Nanobiotechnol. 16, 1–12.
Shome, D., Kalita, D., Jain, V., Sarin, R., Maru, G.B., Bellare, J.R., 2014. Carboplatin loaded polymethylmethacrylate nano-particles in an adjunctive role in retinoblastoma: an animal trial. Ind. J. Ophthalmol. 62, 585.
Sun, H., Choi, D., Heo, J., Jung, S.Y., Hong, J., 2020. Studies on the drug loading and release profiles of degradable chitosan-based multilayer films for anticancer treatment. Cancers 12, 593.
Varshosaz, J., Sarrami, N., Aghaei, M., Aliomrani, M., Azizi, R., 2019. LHRH targeted chonderosomes of mitomycin C in breast cancer: an in vitro/in vivo study. Anti-Cancer Agents Med. Chem. 19, 1405–1417.
Wang, Y., Wang, L., Chen, G., Gong, S., 2017. Carboplatin-Complexed and cRGD-Conjugated Unimolecular Nanoparticles for Targeted Ovarian Cancer Therapy. Macromol. Biosci. 17, 1600292.
Wang, H., Wu, J., Williams, G.R., Fan, Q., Niu, S., Wu, J., Xie, X., Zhu, L.-M., 2019. Platelet-membrane-biomimetic nanoparticles for targeted antitumor drug delivery. J. Nanobiotechnol. 17, 1–16.
White, J.G., 2005. Platelets are covercytes, not phagocytes: uptake of bacteria involves channels of the open canalicular system. Platelets 16, 121–131.
Xu, L., Gao, F., Fan, F., Yang, L., 2018. Platelet membrane coating coupled with solar irradiation endows a photodynamic nanosystem with both improved antitumor efficacy and undetectable skin damage. Biomaterials 159, 59–67.
Xu, P., Zuo, H., Chen, B., Wang, R., Ahmed, A., Hu, Y., Ouyang, J., 2017. Doxorubicin-loaded platelets as a smart drug delivery system: An improved therapy for lymphoma. Sci. Rep. 7, 1–16.
Yang, J., Wang, S., Liu, P., Dai, L., Chen, B., Luan, J., Zhou, J., 2017. Platelet-inspired medicine for tumor therapy. Oncotarget 8, 115748.
Yoo, J.-W., Irvine, D.J., Discher, D.E., Mitragotri, S., 2011. Bio-inspired, bioengineered and biomimetic drug delivery carriers. Nat. Rev. Drug Discov. 10, 521–535.
Zhang, Y., Zhu, X., Chen, X., Chen, Q., Zhou, W., Guo, Q., Lu, Y., Li, C., Zhang, Yu., Liang, D., 2019. Activated platelets-targeting micelles with controlled drug release for effective treatment of primary and metastatic triple negative breast cancer. Adv. Funct. Mater. 29, 1806620.